

Review

## Crystallization Behaviors and Structure Transitions of Biocompatible and Biodegradable Diblock Copolymers

Feifei Xue \* and Shichun Jiang \*

School of Materials Science and Engineering, Tianjin University, Tianjin 300072, China

\* Authors to whom correspondence should be addressed; E-Mails: ffxue@tju.edu.cn (F.X.); scjiang@tju.edu.cn (S.J.); Tel.: +86-022-2740-6647 (F.X.); +86-022-2740-6647 (S.J).

Received: 12 June 2014; in revised form: 10 July 2014 / Accepted: 14 July 2014 /

Published: 4 August 2014

---

**Abstract:** Biocompatible and biodegradable block copolymers (BBCPs) containing crystalline blocks become increasingly important in polymer science, and have great potential applications in polymer materials. Crystallization in polymers is accompanied by the adoption of an extended conformation, or often by chain folding. It is important to distinguish between crystallization in homopolymers and in block copolymers. In homopolymers, chain folding leads to metastable structures introduced by the crystallization kinetics. In contrast, equilibrium chain folding in diblocks can be achieved as the equilibrium number of the folds is controlled by the size of the second block. The structures of BBCPs, which are determined by the competition between crystallization, microphase separation, kinetics and processing, have a tremendous influence on the final properties and applications. In this review, we present the recent advances on crystalline–crystalline diblock copolymer in our group.

**Keywords:** crystalline–crystalline diblock copolymer; biocompatible and biodegradable; crystalline structure

---

### 1. Introduction

The crystallites of polymers adopt either an extended or, what is more common, a chain-folded conformation. It is important to distinguish the crystallization between homopolymers and block copolymers. In homopolymers, chain folding leads to metastable structures as imposed by the crystallization kinetics. On the other hand, chain folding in diblocks is determined by the number of

the folds that can be controlled by the size of the second, non-crystallizable block [1,2]. Coupling and competitive factors among different phase transitions of self-organizing polymers have been widely maneuvered to fabricate ordered structures at different length scales and may hold the key to the development of new structures needed for advanced materials [3]. Multi-scale self-organization of polymers can be plausibly achieved by joining various polymer structures into a block copolymer. For block copolymers that contain crystallizable components the interplay between crystallization and microphase separation somehow strongly influences the structural changes, the morphology, the properties and applications of such materials. Recently, the morphological behaviors of diblock copolymers with at least one crystallizable component have been widely investigated, especially copolymers with one or more biodegradable or/and biocompatible components [4–9].

By covalently linking dissimilar polymer chains in a block copolymer, the immiscibility of the blocks results in a microphase separation of the components, whereby the volume fractions and molecular weights of each block dictate the type and the size of the micro-domains. In the case that one of the blocks can crystallize, the micro-domain morphology provides a unique opportunity to investigate crystallization in confined geometries [10,11]. Meanwhile, a competition between microphase separation and crystallization will lead to major changes in the crystallization kinetics, microstructure and morphology [12–17].

In past years, we focused on two kind of crystalline–crystalline diblock copolymers: poly(ethylene oxide)-*block*-poly( $\epsilon$ -caprolactone) (PEO-*b*-PCL) and poly(ethylene oxide)-*block*-poly(L-lactide) (PEO-*b*-PLA). The PEO-*b*-PCL is a very interesting system since the glass transition temperature  $T_g$ , the crystallization temperature  $T_c$ , and the melting temperatures  $T_m$  of the two components are very similar. On the other hand, PEO-*b*-PLA contains two blocks with distinct  $T_g$ ,  $T_c$  and  $T_m$ . These block copolymers are the ideal system to investigate the nano confinement on the polymer crystallization, and PEO-*b*-PCL could also crystallize on the air–water interface [18,19].

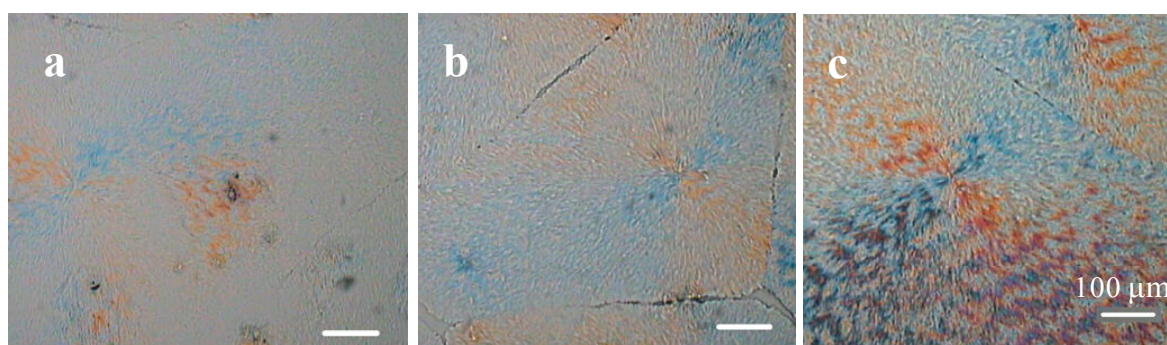
## 2. PEO-*b*-PCL Diblock Copolymers

### 2.1. Crystallization Morphology and Ring-Banded Spherulite of PEO-*b*-PCL Diblock Copolymers [20]

Banding in polymer spherulites, *i.e.*, the presence of radially periodic structure attributable to a twisting of crystallographic orientation about radii that usually give rise to concentric rings or bands of extinction in polarized light microscopy, is a common occurrence and has been studied for more than a century [21]. Banding in polymer spherulites is currently generating renewed interest [21–27]. The banded spherulites that evince a twisting of crystalline orientation about the radii are common in both circumstances and, although occurrence is still quite rare, polymer of both kinds are also found in the form of isolated twisted crystals having roughly the form of right helicoids [21]. Band spacings in polymer spherulites may vary from less than 1  $\mu\text{m}$  to almost 200  $\mu\text{m}$ . Within limits, higher crystallization temperature and moderate rather than high molecular weight tend to yield larger spacings in a given polymer. Ideally, specimens for optical examination should show birefringence still in the gray-white range of interference color, implying a thickness no more than about 10  $\mu\text{m}$  and, in the case of very small band spacings, less if possible [25].

Little work has been done on the morphology of block copolymer with all crystallizable blocks. PEO homopolymer crystallizes in monoclinic form, with alternating right- and left-hand distorted 7/2 helices. PCL crystallizes in an essentially planar zigzag structure [1]. The morphology of double crystalline blocks must be different from that of the homopolymer or the blends of the homopolymers. In the block copolymers, chain connectivity leads to crystalline PEO and PCL lamellae occupying the same crystallite when a comparable fraction of each is present. It leads to the observed large reduction of lamellar thickness and the imperfectness of crystals. Figure 1 shows the optical micrograph of the crystalline morphology of PEO-*b*-PCL diblock copolymer that grew from the melt of the samples prepared from the different solutions observed under crossed polars at 55 °C during the isothermal crystallization process. From the results in Figure 1, it can be concluded that the morphology of PEO-*b*-PCL diblock copolymer depends on the concentration of the solutions prepared for the samples, *i.e.*, the film thickness. The banded spherulites can be observed in Figure 1c; these spherulites display concentric extinction rings.

**Figure 1.** Polarized light micrographs of PEO-*b*-PCL diblock copolymer crystallized at 55 °C from the melt with different film thickness prepared from: (a) 1%; (b) 2%; and (c) 5% (wt %) solutions. The white bar corresponds to 100 μm. Reprinted with permission from Wiley, 2004 [20].



The appearance of rings in the spherulite pattern is dependent on the rate of cooling from the melt; the same polymer can show either a simple extinction by itself or a ring pattern in addition as the conditions of crystallization are changed. It is observed that the ring spacing varies with the temperature of crystallization in polymers. For some polymers, the spacing is larger at lower degrees of supercooling and becomes increasingly smaller as the supercooling is increased. The spherulite patterns of PEO-*b*-PCL diblock copolymer growing at different temperatures are shown in Figure 2. For PEO-*b*-PCL diblock copolymer, with the exception of birefringence of spherulites with a Maltese cross, a distinct pattern of extinction rings absent in pure PEO and PCL is apparent. The average value of periodic distance of extinction rings increases and the ring becomes irregular (Figures 1c and 2f) by increasing the crystallization temperature.

The spherulites were analyzed by digitizing the pattern of the structure. Figure 3 shows the crystallization temperature dependence of the periodic distance of extinction rings, white band and gray band (distance) of the extinction rings in the banding spherulite patterns showed in Figure 2.

**Figure 2.** Polarized light micrographs of PEO-*b*-CPL diblock copolymer crystallized at: (a) 42 °C; (b) 44 °C; (c) 46 °C; (d) 48 °C; (e) 50 °C; (f) 52 °C from the melt with the films prepared from 5% (wt %) solutions. The white bar corresponds to 50 μm. Reprinted with permission from Wiley, 2004 [20].

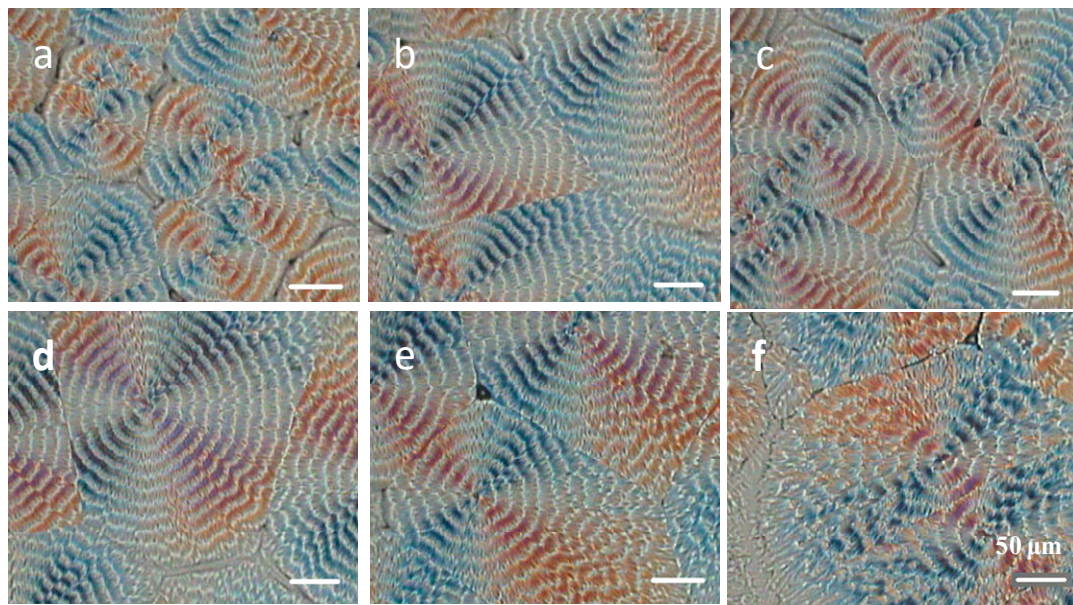
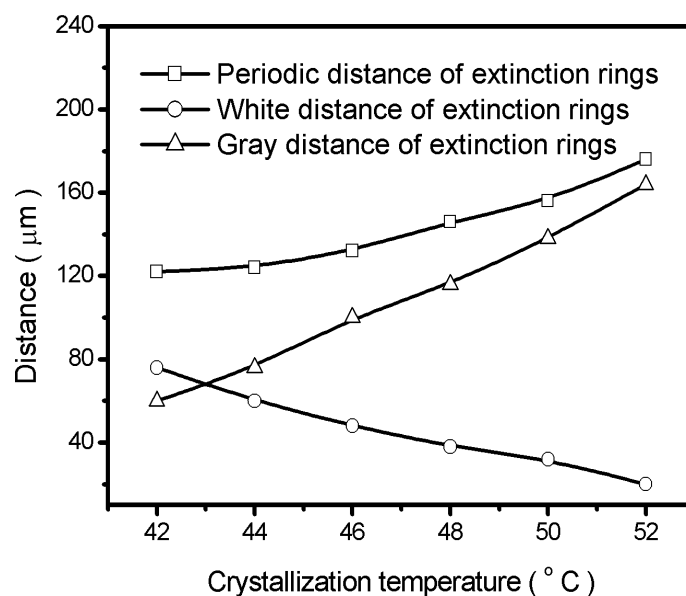


**Figure 3.** Variation of distance extinction rings with crystallization temperature for PEO-*b*-PCL diblock copolymer. Reprinted with permission from Wiley, 2004 [20].



It can be seen that the periodic distance and the gray distance of the extinction rings increase with crystallization temperature; however, the white distance of the extinction rings decreases with the crystallization temperature. The most comprehensive study on the ring-banded spherulite structures in homopolymers such as polyethylene has been published by Keith and Padden [24]. The proposed basic mechanism leading to the ring pattern is axial twisting in lamellae under the influence of surface stress, and cooperative arrangement of twisted crystallites. Moreover, these conclusions have also been used to

explain the formation of ring-banded spherulites in the mixtures. Wang and coworkers [26] have pointed out that the formation of ring-banded spherulites in polymer mixtures is connected with crystallization kinetics. However, how the general mechanism leading to this peculiar texture has not yet been clarified. For the present case, the formation of ring-banded spherulites of crystalline–crystalline diblock copolymer is more complex. According to the results in Figure 3 and the crystallization behaviors of PEO and PCL blocks in the block copolymer, we know that the white band in the spherulite corresponds to the PEO block and the gray ring related to the PCL block in Figure 2. It can be seen that the PEO block is the main reason for the formation of the ring-banded spherulites in the PEO-*b*-PCL double crystalline diblock copolymer. Schacht and coworkers [28] reported that in the temperature from 15 to 25 °C for the PEO-*b*-PCL block copolymer, both PCL and PEO constituents crystallize. The PCL constituent crystallizes first, before reaching the temperature of crystallization,  $T_c$ , or at the onset of the isothermal step. Next, the PEO constituent crystallizes isothermally. When the crystallization temperature is modified from 30 to 42 °C, only the PCL constituent crystallizes during the isothermal step. Figure 1 indicates that the ring-banded spherulite depends on the thickness of the film for POM observation. The banded morphology in PEO-*b*-PCL diblock copolymer is formed due to the density fluctuation of melting block copolymer.

## 2.2. Crystallization Transitions in PEO-*b*-PCL Diblock Copolymers [29]

Because of the chain connectivity of the block copolymers, crystalline/crystalline PEO and PCL lamellae occupied the same crystallite when comparable fractions of each were present, thereby leading to the observed large reduction of lamellar thickness, the imperfectness of crystals (as evidenced by the melting temperature depression) and the conforming to the wide angle X-ray scattering (WAXS) patterns for the presence of coexisting crystalline components. The final solid-state structure in a semicrystalline block copolymer is as well a matter of the interplay between microphase separation and crystallization [30–32]. When a crystallizable component is confined within a large number of small isolated microdomains, a substantial decrease in crystallinity as compared to the corresponding homopolymers can sometimes be observed as a result of larger supercooling that are required for crystallization as well as the topological restrictions caused by the confinement. The factors that affect the crystallization properties of PEO-*b*-PCL block copolymers have been reported and typically depend on the block length and the crystallization temperature [33–35]. Intuitively, the block with higher molecular weight crystallizes first in PEO-*b*-PCL crystalline–crystalline diblock copolymers whereas there are not any relevant reports on following the crystallization process of a symmetric diblock copolymer.

To elucidate the nature of the single melting peak of the symmetric double crystalline blocks of PEO-*b*-PCL copolymer, the structure and the structure transition behavior of the copolymer were investigated by time-resolved synchrotron simultaneous WAXS/ small angle X-ray scattering (SAXS). The scattering patterns were collected in time frames of 10 and 60 s for isothermal crystallization temperatures at 40 and 50 °C, respectively. The calibration of the spacings for the different detectors and positions was made as follows: the diffraction peaks of a crystalline PET sample were used for the WAXS detector and the different orders of the long spacing of rat tendon tail ( $L = 65$  nm) were used for the SAXS detector.

Typical time-resolved SAXS and WAXS profiles obtained during isothermal crystallization of PEO<sub>5k</sub>-*b*-PCL<sub>5k</sub> at 40 °C are shown in Figure 4a,b, respectively. The relative low supercooling for PEO-*b*-PCL block copolymer crystallization resulted in a relative low crystallization rate, allowing the possibility of the detailed examination of simultaneously collected SAXS and WAXS profiles. One can see from Figure 4 that a detectable scattering shoulder first appears in the raw SAXS profile is almost at the same time as the crystalline reflections (WAXS) first become identifiable. The SAXS results in Figure 4a imply the long spacing is almost constant during the isothermal crystallization, and the results in Figure 5 indicate that the PEO block crystallizes first.

**Figure 4.** Simultaneous SAXS (a) and WAXS (b) profiles collected during isothermal crystallization of PEO-*b*-PCL at 40 °C. Reprinted with permission from Springer, 2008 [29].

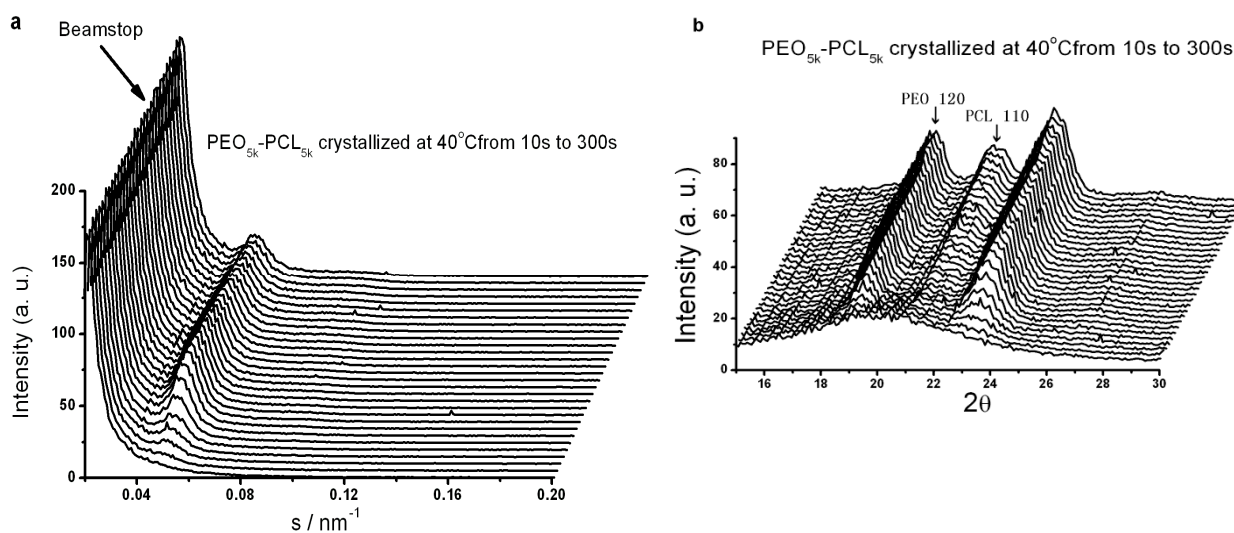
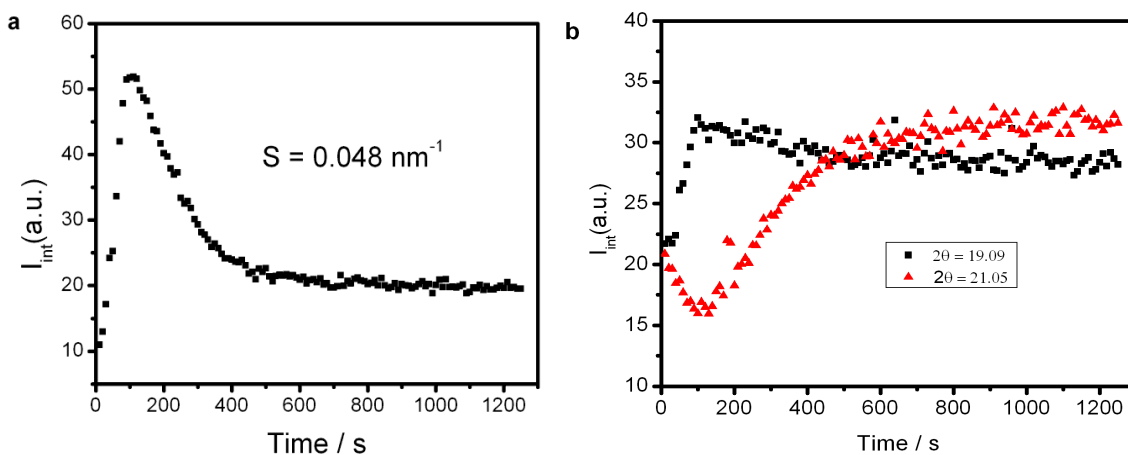


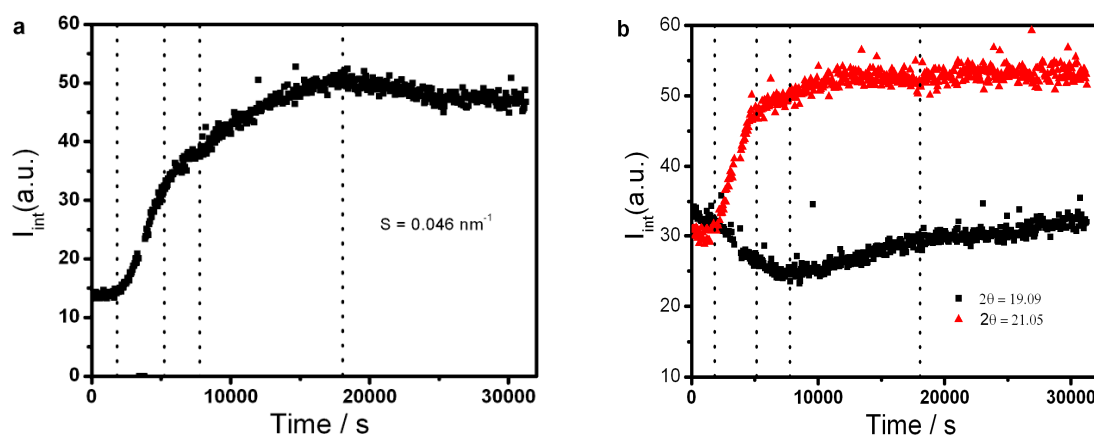
**Figure 5.** The integrated intensity  $I_{int}$  as a function of time obtained from (a) SAXS and (b) WAXS measurements during isothermal crystallization of PEO-*b*-PCL at 40 °C. Reprinted with permission from Springer, 2008 [29].



It is reported that peaks corresponding to a lamellar repeat were present in the supercooled melt (by SAXS) prior to the observation of three-dimensional crystal ordering (by WAXS), and the lag time ( $t_{WAXS} - t_{SAXS}$ ) decreases with a decrease in crystallization temperature or increase in the degree of

supercooling. Wang *et al.* discussed the different detection limits of SAXS and WAXS [36]. They argued that the detection limits of SAXS and WAXS are different and to detect the presence of the initial crystalline phase, by merely comparing the first appearance of SAXS and WAXS intensities, therefore may not provide meaningful information. They thought that since the crystallinity in the early stages is low, the WAXS technique may not be able to detect it. By contrast, the lower fraction of crystallinity can be readily detectable by SAXS as long as the contrast between the constituting phases is sufficient and the length scale is within the detectable range. However, that is not the case for the PEO-*b*-PCL block copolymer as shown in Figures 5 and 6.

**Figure 6.** The integrated intensity  $I_{\text{int}}$  as a function of time obtained from (a) SAXS and (b) WAXS during isothermal crystallization of PEO-*b*-PCL at 50 °C. Reprinted with permission from Springer, 2008 [29].



The time-resolved SAXS and WAXS profiles were also investigated during isothermal crystallization of PEO<sub>5k</sub>-*b*-PCL<sub>5k</sub> at 50 °C, and the time evolution of the integrated intensity from the scattering maximum ( $s = 0.046 \text{ nm}^{-1}$ ) of SAXS profiles and strong reflections ((120) of PEO and (110) of PCL at  $2\theta = 19.09$  and  $21.05$ , respectively) of WAXS profiles are shown in Figure 6a,b, respectively. The lower supercooling for PEO-*b*-PCL block copolymer resulted in a lower crystallization rate, allowing the more detailed examination of simultaneously collected SAXS and WAXS profiles, which can be compared with the results obtained at 40 °C. It is worth noting that PCL block crystallizes first upon PEO<sub>5k</sub>-*b*-PCL<sub>5k</sub> crystallization at 50 °C as shown in Figure 6. One can find that all of the transitions of the PEO-*b*-PCL crystallization process take place at the same time for both SAXS and WAXS for the block copolymer crystallized at 50 °C, which indicates both the nano- and micro- scale structure transformations relate to the PEO and PCL block crystallization behavior and the block copolymer condensate structures.

The transition at different crystallization temperatures of PEO-*b*-PCL has been investigated during the crystallization process. A temperature-dependent reversible crystallization behavior is illustrated. The transitions of PEO-*b*-PCL diblock copolymer during molten crystallization can be detected from the layer scale to crystal scale by SAXS and WAXS at the same time. The time-resolved  $I_{\text{int}}$  is proportional to the product of volume fraction for the PEO and PCL phase ( $\phi_{\text{PEO}}, \phi_{\text{PCL}}$ ) and the scattering contrast due to the electron density difference  $(\rho_{\text{PEO}} - \rho_{\text{PCL}})^2$  during the block copolymer crystallization.

### 2.3. Soft Nanoconfinement on the Crystallization Behavior of PEO-*b*-PCL Diblock Copolymers [37]

Confinement of polymer crystallization is gaining considerable attention with the development of micro- and nano- science and technology. Confined polymer crystallization is usually investigated through the crystalline polymers in confined environments, such as block copolymers, inorganic/polymer hybrid and polymer blends. The simple and effective way to study nano-confined polymer crystallization is to use crystalline–amorphous diblock copolymer as templates. A remarkable property of block copolymer is their ability to self-assemble in the melt into a variety of ordered structures with nanoscale periodicities via a microphase separation process [38–42]. Microphase separation is driven by the enthalpy of demixing the constituent components of the block copolymers, whilst macrophase separation is prevented by the chemical connectivity of the blocks. These structures can be controlled by varying the composition of the block copolymer or the segregation between blocks (via temperature or degree of polymerization). In addition to the now well-established lamellar, hexagonal-packed cylinder and body-centered cubic micelle phase, a number of new morphologies have been discovered, which supplement the “classical” structures. To date there have only been a limited number of studies of the kinetics of ordering block copolymers. In part, this may be due to the necessity for measurements of structure development with a high temporal resolution. Experiments of the time evolution of structure in microphase-separated block copolymers can be carried out using synchrotron small-angle X-ray scattering. An early study of the ordering of an asymmetric PS-*b*-PB diblock onto a cubic lattice was performed by Harkless *et al.* following a quench from the disordered phase; the development of the ordered structure was monitored using SAXS with a time resolution of 1–3 s. The development of a structure factor peak from an ordered liquid of PS spheres was observed initially. At later times, the liquid peak decayed as the first-order Bragg peak from a BCC lattice developed. The measured intensity of the Bragg peak is proportional to the fraction of ordered material in the sample [36].

The structure and the structure transition behavior of the copolymer were investigated by time-resolved synchrotron simultaneous WAXS/SAXS. The scattering patterns were collected in time frames of 10 and 60 s for isothermal crystallization temperatures at 40 and 50 °C under different conditions, which would be helpful to observe the confined crystallization behavior at lower crystallization temperature and the detail on the structure transition at higher crystallization temperature.

Typical time-resolved WAXS and SAXS profiles obtained during isothermal crystallization of PEO<sub>5k</sub>-*b*-PCL<sub>1k</sub> and PEO<sub>5k</sub>-*b*-PCL<sub>30k</sub> at 40 °C after melting at 80 °C are shown in Figures 7 and 8, respectively. The WAXS results (Figure 7) indicate that there is only the crystallization behavior of the blocks with higher molecular weight in the diblock copolymers for the investigated samples. As shown in Figure 7 of the WAXS patterns, the intensity of amorphous halo decreased and the crystalline peaks appeared with time. The WAXS results in Figure 7 illustrate that the change of the scattering intensity origin is from only one block crystallization of PEO or PCL block in the copolymers and there is no change of crystalline forms both for PEO and PCL in the asymmetric diblock copolymers during the crystallization. In the later stage of crystallization, the long period peak appeared in the SAXS profiles (Figure 8a,b), after some induction period, suggests that there are lamellar structures almost without long space changing during structure transition due to the crystallization of the block copolymer quenched from melt. The SAXS profiles obtained from the

asymmetric block copolymer crystallized at 40 °C indicate that the stacked lamellar structure formed very fast, for PEO<sub>5k</sub>-*b*-PCL<sub>1k</sub> and PEO<sub>5k</sub>-*b*-PCL<sub>30k</sub> are only 20 s and 50 s, respectively. It is difficult to analyze the confined crystallization behavior and the structure formation of the investigated asymmetric block copolymers at the earlier stage from the obtained results of simultaneous SAXS and WAXS measurements at 40 °C. The measurements for detail analysis on the structure formation at an early stage were performed at a higher temperature.

**Figure 7.** Time-resolved WAXS profiles of block copolymers obtained at 40 °C after cooling from 80 °C. Reprinted with permission from Wiley, 2012 [37].

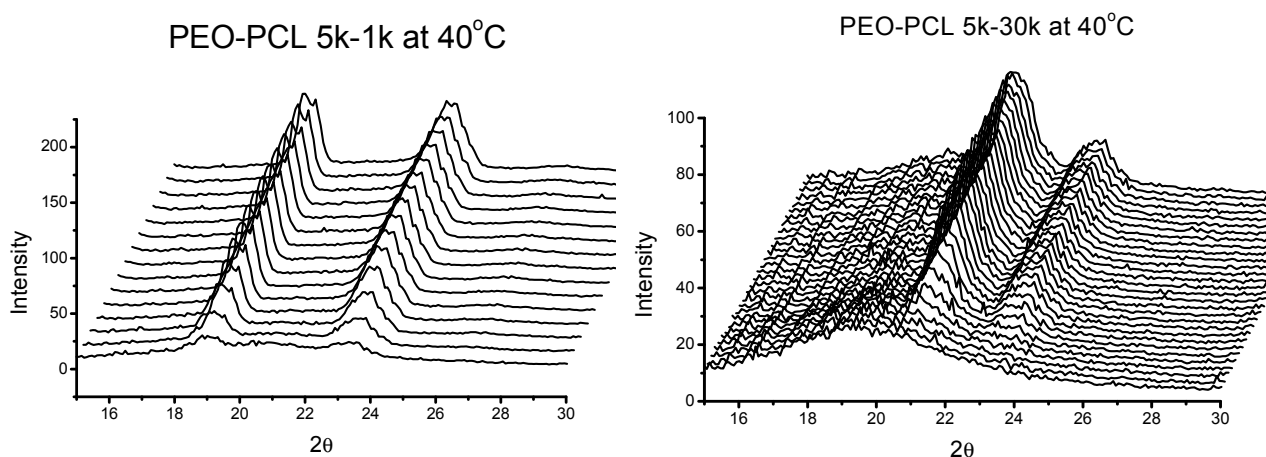
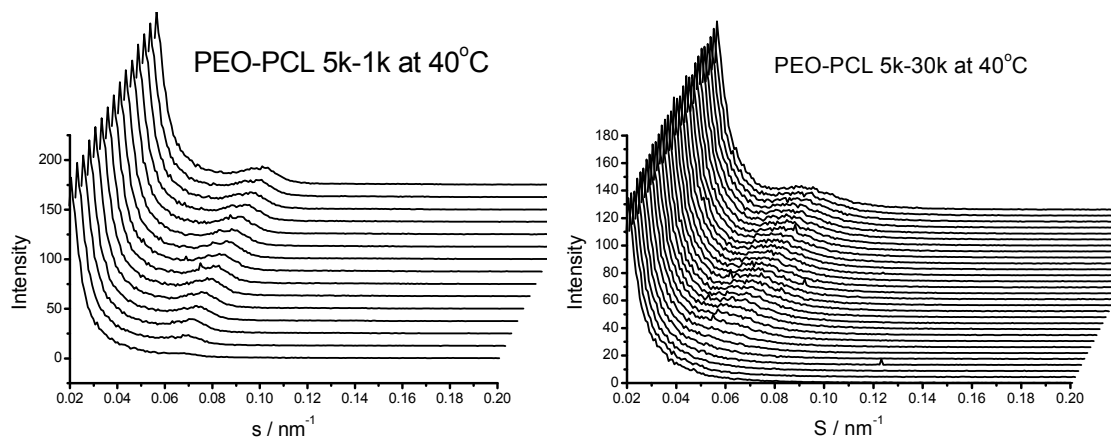


**Figure 8.** Time-resolved SAXS profiles of block copolymers obtained at 40 °C after cooling from 80 °C. Reprinted with permission from Wiley, 2012 [37].



The crystallization behaviors of the asymmetric diblock copolymers crystallized at 50 °C were recorded via synchrotron simultaneous SAXS/WAXS for the investigation of nano confined crystallization behavior in detail. Figure 9 shows the observed SAXS profiles ( $I(s)$  vs.  $s$ ) detected in the earlier time region immediately after the temperature jump. Here we do not find reasonable ground to assume that the density fluctuation may occur in the melt of the asymmetric block copolymer, and some denser regions start to grow to form domains, but rather these domains may be isolated from each other. After a certain amount of time, these domains gather together, and finally, a stacked lamellar structure may be formed from these domains. To check this natural structure evolution, we analyzed the SAXS data on the basis of (i) the Guinier plot in the earlier time region where isolated domains are formed, (ii) the

Debye–Bueche plot in the time region where the correlation of the two domains becomes stronger, and (iii) the correlation function in the later stage to estimate the stacked lamellar structure.

The time evolution of the integrated intensity obtained from the scattering maximum ( $s = 0.049$  and  $0.051 \text{ nm}^{-1}$ ) of SAXS profiles measured from the asymmetric diblock copolymers at  $50 \text{ }^\circ\text{C}$  are shown in Figures 10a and 11a (The inset results obtained from pure PEO and PCL). The strong reflections ((120) of PEO at  $2\theta = 19.09^\circ$  and (110) of PCL at  $2\theta = 21.05^\circ$ , respectively) of WAXS profiles obtained diblock copolymers and homopolymers are shown in Figures 10b and 11b.

**Figure 9.** Time-resolved SAXS profiles of block copolymers obtained at  $50 \text{ }^\circ\text{C}$  after cooling from  $80 \text{ }^\circ\text{C}$  for the initial 30 min. Reprinted with permission from Wiley, 2012 [37].

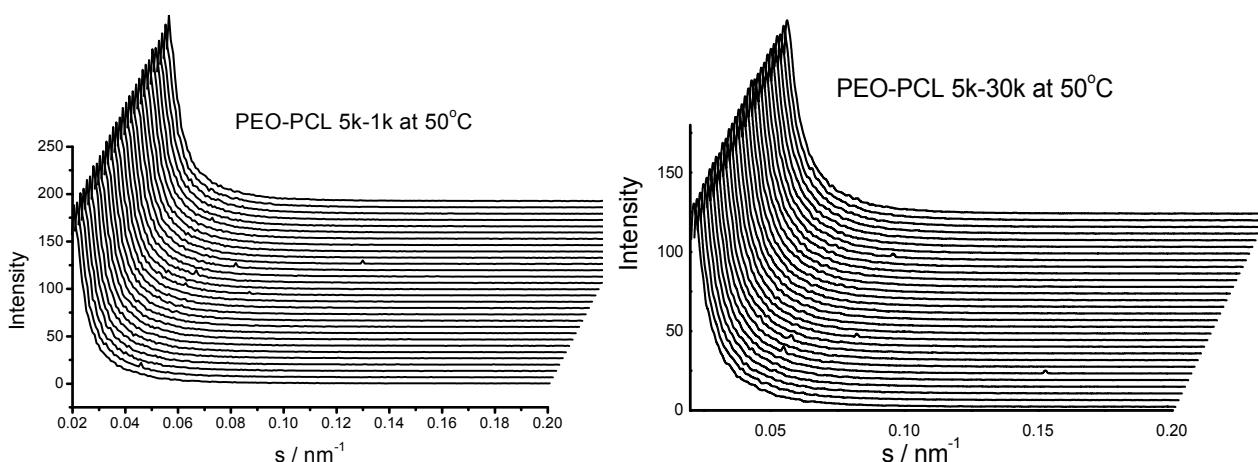


**Figure 10.** Time evolution of the integrated intensity obtained from SAXS/WAXS of  $\text{PEO}_{5k}\text{-}b\text{-PCL}_{1k}$  asymmetric block copolymer and pure PEO at  $50 \text{ }^\circ\text{C}$ . Reprinted with permission from Wiley, 2012 [37].

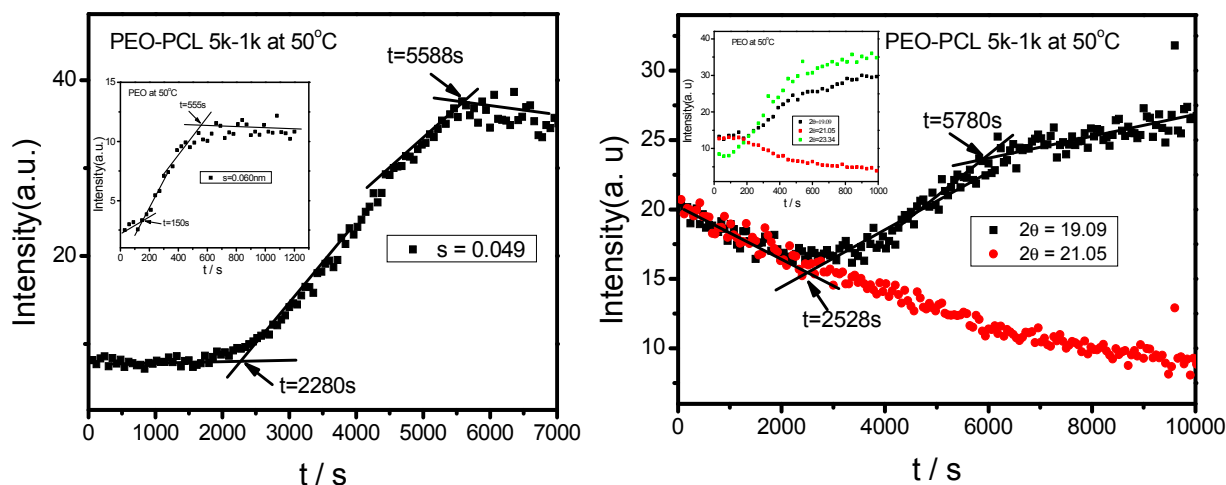
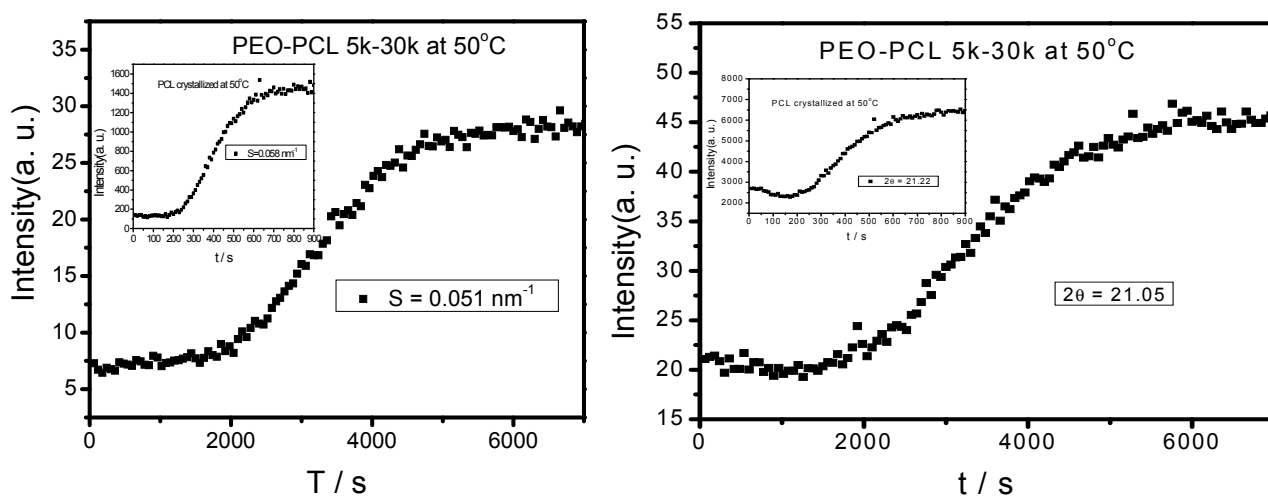


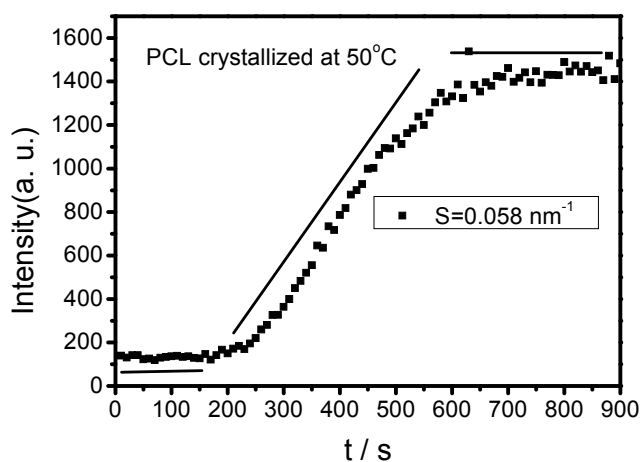
**Figure 11.** Time evolution of the integrated intensity obtained from SAXS/WAXS of PEO<sub>5k</sub>-PCL<sub>3k</sub> asymmetric block copolymer and pure PCL at 50 °C. Reprinted with permission from Wiley, 2012 [37].



Comparing the crystallization behavior of pure PEO and PCL with that of PEO block and PCL block in the diblock copolymers observed via SAXS/WAXS, one can find that the crystallization kinetics of the crystalline blocks are much lower than that of pure polymers. In order to investigate the crystallization kinetics behavior observed by SAXS/WAXS, characteristic crystallization rate ( $\nu^*$ ) is introduced. Figure 12 shows the time-dependent integrated intensity obtained from SAXS of PCL isothermally crystallized at 50 °C. It is obvious that the integrated scattering intensity as a function of time exhibits three stages. The first stage is the time to induce crystallization; the second one is the time of growth; and during the last one, the crystallization is terminated. The slope ( $k$ ) of the time related scattering intensity obtained from the second stage can be used to characterize the crystallization kinetics.

$$\nu^* \propto k \tag{1}$$

**Figure 12.** Time related integrated intensity obtained from SAXS of pure PCL at 50 °C. Reprinted with permission from Wiley, 2012 [37].



The quotient  $Q = v_{\text{home}}^* / v_{\text{cop}}^*$  is used to value the crystallization behavior of homopolymers and the diblock block copolymers. It is difficult to obtain  $Q_{\text{PEO}}$  at 40 °C, because the crystallization is too fast to be tracked by synchrotron SAXS/WAXS with the limited cooling rate from high temperature.  $Q_{\text{PCL}} = 10$  at 40 °C.  $Q_{\text{PEO}} = 3$  and  $Q_{\text{PCL}} = 500$  at 50 °C. When  $Q = 1$ , the crystallization of the crystalline block in the diblock copolymer is not affected. The bigger  $Q$ , the more effect on the crystallization behavior can be found in the asymmetric diblock copolymers. Therefore, the PEO block has more effect on the PCL crystallization behavior in the present observed asymmetric diblock copolymers at least at 50 °C. The confinement on the crystallization behavior in the asymmetric diblock copolymers may be due to the chemical structure of the copolymers and the crystalline property of the blocks. The molecular weight of the blocks in the present investigated asymmetric diblock copolymers is different. The crystallization of PEO block in the copolymer is in the confinement of PCL block with 1 k molecular weight; however, the crystallization of PCL block in the copolymer is in the confinement of PEO block with 5 k molecular weight. On the other hand, there is a much higher molecular weight of the whole copolymer for the crystalline PCL than that for the crystalline PEO.

#### 2.4. Confined Crystalline Lamella Formation in PEO-*b*-PCL Diblock Copolymers [43]

The understanding of the complicated properties of double crystalline diblock copolymers is still in a nascent stage despite the number of prior reports that have been published. The reported results show that depending on crystallization temperature, various crystallization behaviors are involved during the crystallization process and lamellae could be found for all of the observed samples. It is interesting to observe, by synchrotron simultaneous SAXS and WAXS, that the multi-scale transitions can be detected at the same time.

The simultaneous synchrotron SAXS/WAXS results were recorded at the same time when the temperature cooled to the pre-setted isothermal crystallization temperature. Figures 13 and 14 show the obtained SAXS and WAXS results of the four measured samples, respectively. The observable scattering maximum intensity related  $s$  ( $s = 2\sin\theta/\lambda = q/2\pi$ ) values of the measured samples shown in Figure 13 are 0.058, 0.056, 0.053 and 0.056 for PEO<sub>5k</sub>-*b*-PCL<sub>3k</sub>, PEO<sub>5k</sub>-*b*-PCL<sub>10k</sub>, PEO<sub>5k</sub>-*b*-PCL<sub>15k</sub>, and PEO<sub>5k</sub>-*b*-PCL<sub>20k</sub>, respectively. Time-dependent scattering intensity of related  $s$  for different samples is shown in Figure 15. From the results in Figure 15, one can find that the scattering intensity of the measured asymmetric crystalline–crystalline diblock copolymer increases with the isothermal crystallization time, which is different from that of PEO<sub>5k</sub>-*b*-PCL<sub>5k</sub> symmetric crystalline–crystalline diblock copolymer. To investigate the crystalline structure of the these diblock copolymers, the time-dependent scattering intensity of the typical diffraction peaks of PEO<sub>(120)</sub> and PCL<sub>(110)</sub> are shown in Figure 16. The results in Figure 16 imply that the block in the crystalline–crystalline diblock copolymers with higher molecular weight crystallizes first and faster than the other block with the lower molecular weight.

**Figure 13.** Time-resolved SAXS profiles of block copolymers obtained at 40 °C after cooling from 80 °C. Reprinted with permission from Springer, 2013 [43].

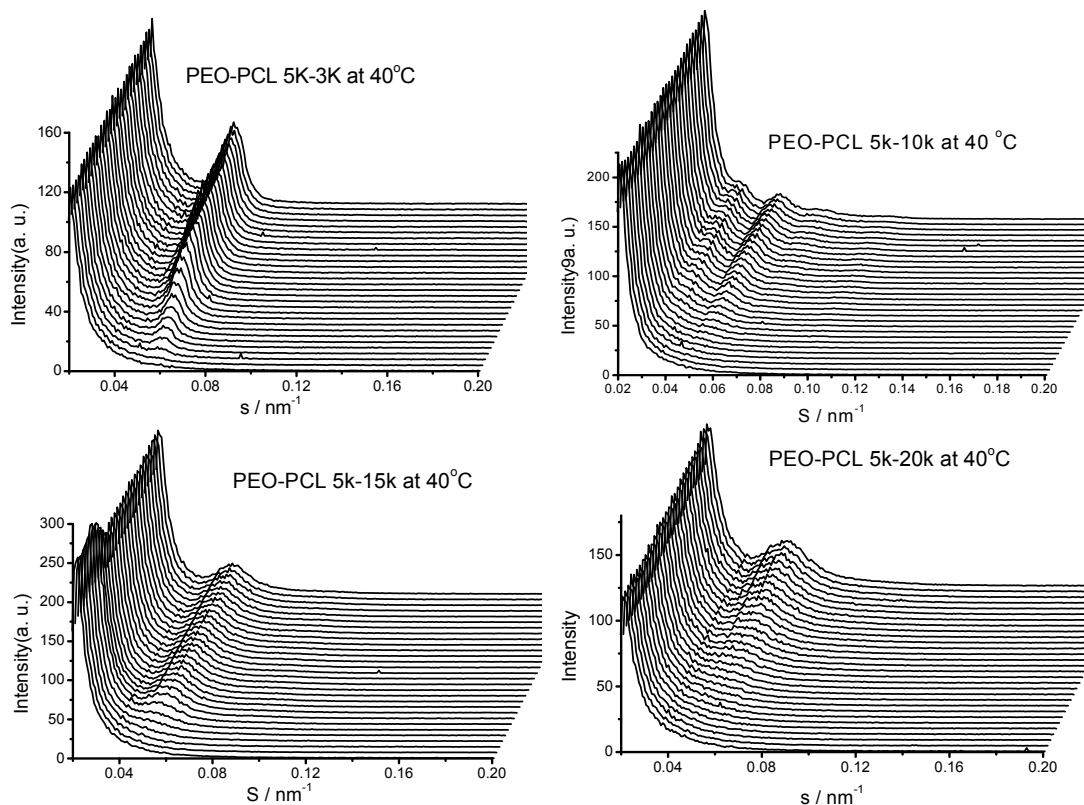


**Figure 14.** Time-resolved WAXS profiles of block copolymers obtained at 40 °C after cooling from 80 °C. Reprinted with permission from Springer, 2013 [43].

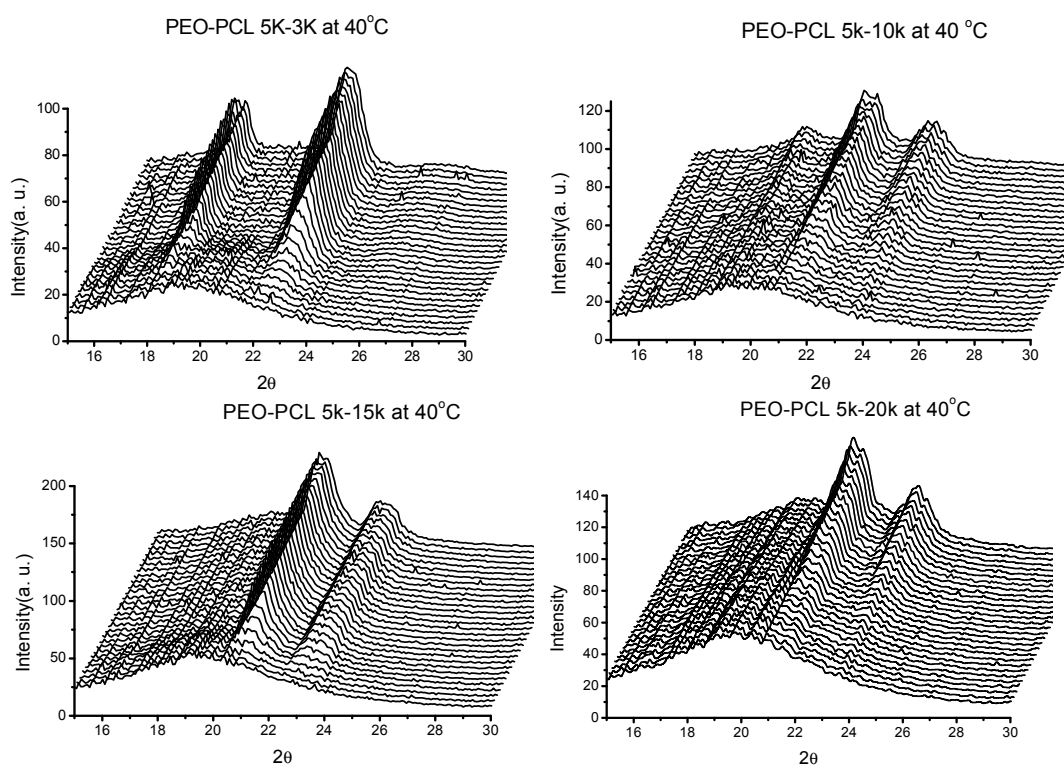


**Figure 15.** Time-dependent normalized scattering intensity of SAXS. Reprinted with permission from Springer, 2013 [43].

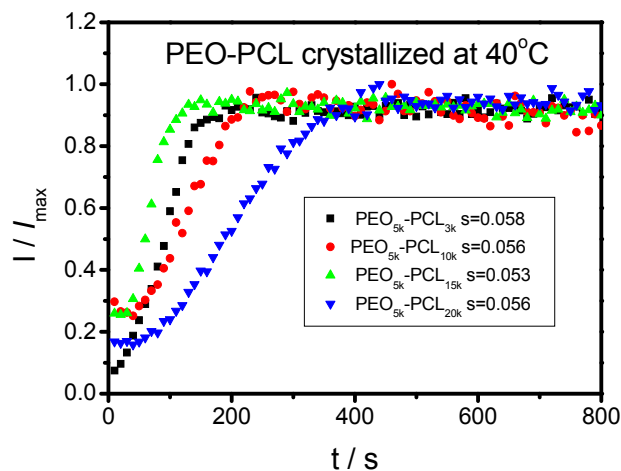
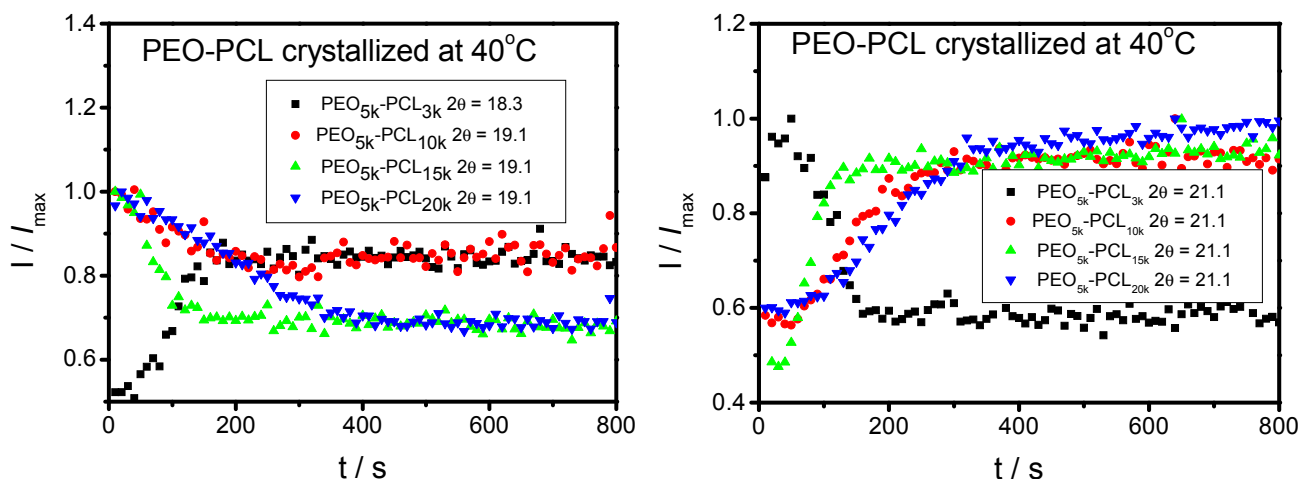
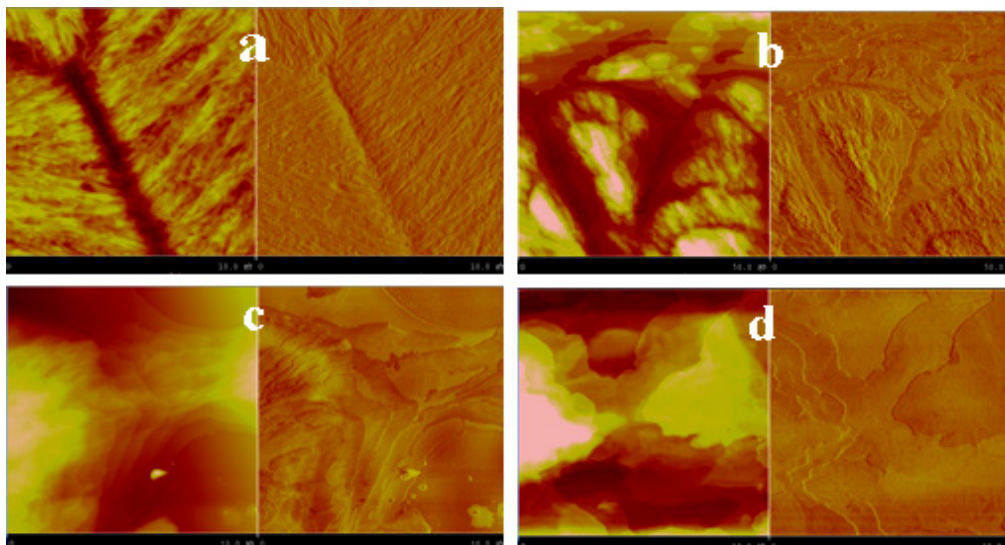


**Figure 16.** Time-dependent normalized scattering intensity of WAXS. Reprinted with permission from Springer, 2013 [43].



The SAXS results of the isothermal crystallization of the diblock copolymers may indicate the formation of lamellar solid-state structures. To confirm the final structure of the block copolymers, atomic force microscopy (AFM) observations were performed, and the obtained images are shown in Figure 17. The layer of the crystal seen in all of the AFM images indicates that final structure of the crystalline–crystalline asymmetric diblock copolymers is determined by the crystallization behavior of the blocks to overwrite the microphase separation behavior, which induced microdomains and formed lamellar structures. The formation of lamellar structures of the crystalline–crystalline diblock copolymer with alternating layers of amorphous and crystalline was expected according to the SAXS and AFM results.

**Figure 17.** AFM height (left) and phase (right) images ( $10\ \mu\text{m} \times 10\ \mu\text{m}$ ) of the final morphologies of the asymmetric diblock copolymers (a) PEO<sub>5k</sub>-*b*-PCL<sub>3k</sub>; (b) PEO<sub>5k</sub>-*b*-PCL<sub>10k</sub>; (c) PEO<sub>5k</sub>-*b*-PCL<sub>15k</sub>; and (d) PEO<sub>5k</sub>-*b*-PCL<sub>20k</sub>. Reprinted with permission from Springer, 2013 [43].

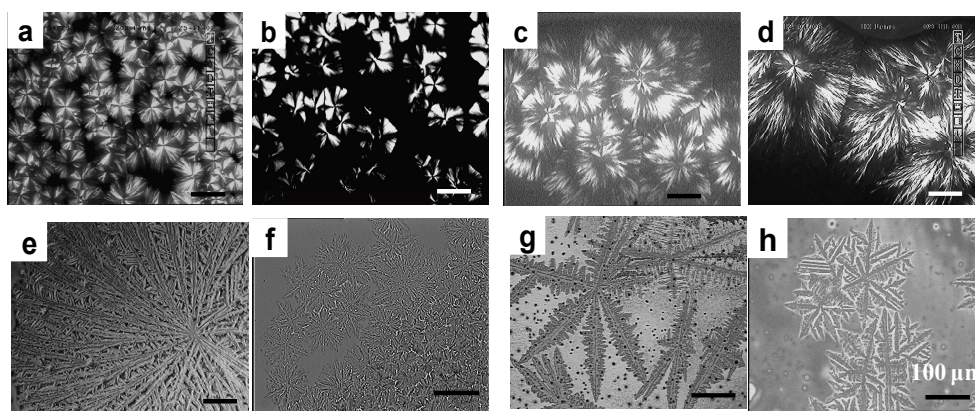


### 3. PEO-*b*-PLA Diblock Copolymers

#### 3.1. Soft Confined Crystallization and Microphase Separation-Determined Morphologies of PEO-*b*-PCLA Diblock Copolymers [7]

PEO-*b*-PLA diblock copolymer films several microns thick were completely melted at 180 °C, and then quickly cooled to the temperatures ( $T_c$ ) for isothermal crystallization. After complete crystallization, the films were cooled to room temperature rapidly. The morphologies were observed using polarized optical microscope at room temperature. General spherulites were observed in the copolymer films isothermally crystallized at 90 °C and 100 °C as shown in Figure 18a,b. Figure 18c showed that banded spherulite was formed, when crystallized at 110 °C from the disordered state. An interesting morphology of which the center is spherulite and the outer is dendrite was formed at  $T_c = 115\ \text{°C}$  shown in Figure 18d. When crystallized at a higher temperature,  $T_c > 115\ \text{°C}$ , the crystallization behavior and the crystalline morphologies are absolutely different from those at low  $T_c$  [7,44–47]. Dense dendrites were formed at 120 °C, as shown in Figure 18e,f; the morphologies composed by the main branches were star-shaped, and the second branches grew along the main branches. At even higher  $T_c$ , the dendrite and fractal dendrite were formed, as shown in Figure 18g at 125 °C and Figure 18h at 130 °C. The morphologies composed by the main branches are still star-shaped, but the number of the main branch is much smaller than that of dense branches. Furthermore, the morphologies formed at 130 °C are more regular, which are composed of six main branches, and the second branches grow along the main branches, the second branches along one main branch are parallel with each other, then the third branches grow in the same way as the second branches. The peculiar dendrite formed in high temperature range can be explained with nucleation, diffusion, growth, and their competition with each other and the addition of PEO block [7,44,48].

**Figure 18.** Morphologies of PLLA<sub>16k</sub>-*b*-PEO<sub>5k</sub> copolymer films isothermally crystallized at (a) 90 °C; (b) 100 °C; (c) 110 °C; (d) 115 °C; (e) 120 °C; (f) 120 °C; (g) 125 °C; and (h) 130 °C. The bar corresponds to 100 μm. Reprinted with permission from Wiley, 2008 [7].



As shown in Figure 18, the morphologies of the diblock copolymer are crystallization temperature ( $T_c$ ) dependent. The morphologies evaluate from radial spherulite, banded spherulite at low  $T_c$ , to dense branches, dendrite and fractal dendrite at high  $T_c$ . It has been reported that the crystallization behavior of PLA can be classified into the low and high temperature ranges based on the crystallization modification, nucleation, and growth rate [7,44,47,49–54], but such distinguished morphological evolution with  $T_c$  has never been investigated. We speculated that the  $T_c$ -dependent morphological behavior of the asymmetric copolymers is the result of soft confinement crystallization. It has been confirmed that the PEO-*b*-PLA copolymers are disordered in the melt [6,10,55]; the two components, PLA and PEO blocks, are weakly segregated. Microphase separation of the copolymers is driven by the crystallization of PLA block, which will influence the diffusion PLA component, growth and orientation of PLA lamellae. Consequently, dendrites are formed at high crystallization temperature range [10]. However, the state of PEO block is melted during the whole crystallization process, and the volume fraction of PEO block is small (<25%). As a consequence, the confinement of the microdomains formed by microphase separation on the crystallization of PLA is weak. Although the amorphous PEO phase influences the diffusion of the PLA component, growth, and orientation of the PLA lamellae, the PLA component is still able to diffuse across the amorphous PEO layer to the growth front. Consequently, the crystallization of the PLA block overwrites the former structure formed by microphase separation, and the morphological features are of  $T_c$  dependence, not dominated by structure formed by microphase separation.

A synchronous SAXS was employed to explore the structural change with various annealing temperatures from the melt. SAXS data was obtained via scanning the samples at the temperature with 30 s exposure annealed from the disordered melt. All of the data were corrected for background scattering before analysis and treated with software Fit 2D. Figure 19a shows the SAXS patterns of PLA<sub>16k</sub>-*b*-PEO<sub>5k</sub> copolymers isothermal at 130, 120, 110 and 100 °C from the disordered state. Scattering peaks can be seen in SAXS patterns, indicating that disorder to order transition occurs. That is microphase separation driven by crystallization of PLA block. The positions of scattering peak for PEO-*b*-PLA copolymer shift to smaller  $q$ , indicating the long periods in the copolymers are larger than that in PLA homopolymer. Furthermore, Figure 19a also shows that the long period for PLA<sub>16k</sub>-*b*-PEO<sub>5k</sub> copolymer becomes larger with  $T_c$  increasing in the temperature range from 110 to

130 °C. Meanwhile, the long period at 100 °C is larger than that at 110 °C and the value of the long period at 100 °C is nearly the same with that at 120 °C. In the high crystallization temperature range (110–130 °C), the crystallization of PLA block predominates the crystal structure, the lamellar thickness increases with  $T_c$ , which results in the increase of the long period with  $T_c$ . In the low crystallization temperature range, the influence of microphase separation on the crystal structure becomes stronger. Consequently, the long period at 100 °C is larger than that at 110 °C.

**Figure 19.** SAXS patterns of PLLA<sub>16k</sub>-*b*-PEO<sub>5k</sub> copolymer (a) isothermally crystallized at 130, 120, 110, 100 °C from the melt (b) the isothermal process at 100 °C annealed from the melt.

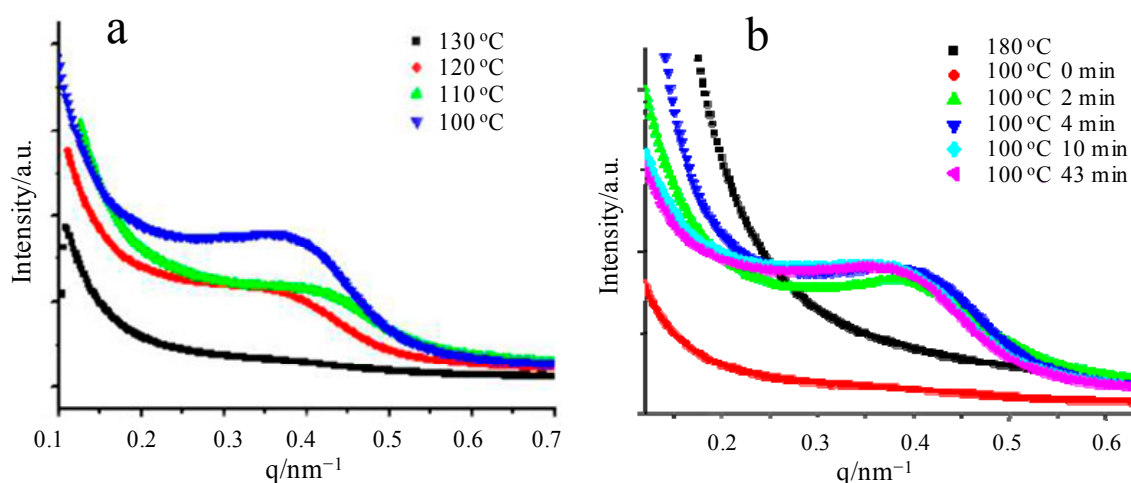
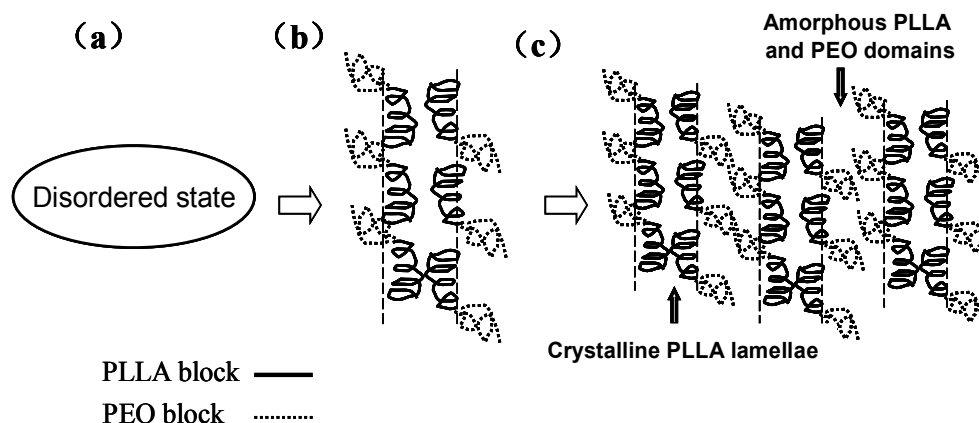


Figure 19b shows the SAXS patterns of PLA<sub>16k</sub>-PEO<sub>5k</sub> copolymer in the annealing and isothermal processes. The copolymer is melted at 180 °C, and then cooled to 100 °C; there is a small scattering peak in the SAXS pattern labeled 100 °C 0 min in Figure 19b, indicating that disordered to order transition occurs, which is driven by crystallization of PLA block. This has been confirmed by SAXS, as shown in Figure 19a. The following isothermal process shows the structural change in the process of crystallization. The increase of the intensity and the long period indicate the crystallization growth of PLA.

On the basis of the morphological features in Figure 18 and the SAXS data in Figure 19, the microstructure during phase transition in a soft environment can be schematically illustrated in Figure 20. The copolymer system is disordered in the melt state shown in Figure 20a. Crystallization of PLA block drives microphase separation of the copolymer, and then alternate amorphous–crystalline phase structure is formed, the microstructure can be shown in Figure 20b. Because of the weak confinement of the microdomain on the diffusion and crystallization growth, the crystallization will breakout the confinement, overwrite the microstructures formed by microphase separation, and a new morphology is formed. The amorphous PEO and PLA blocks are distributed between the interfaces of PLA crystals and the surfaces, as schematically shown in Figure 20c.

**Figure 20.** A schematic illustration of phase transition of the asymmetric PLLA-*b*-PEO copolymers in a soft environment: (a) disordered state; (b) micro-structures formed by microphase separation and the crystallization of PLLA block; and (c) the final morphological structure.



### 3.2. Hard Confined Crystallization and Microphase Separation-Determined Morphologies of PEO-*b*-PCLA Diblock Copolymers [7]

Figure 21 shows the morphologies of PLA<sub>16k</sub>-*b*-PEO<sub>5k</sub> copolymer films formed with cold crystallization and in a hard environment. For cold crystallization, the copolymer films were cooled from the melt state, and then isothermally crystallized at very low temperature. Dense-distributed small spherulites are observed at 55, 60, 70 °C and 80 °C as shown in Figure 21a–d, respectively. Microphase separation of the copolymer may occur driven by the immiscibility of PLA and PEO blocks at low temperatures. However, the microdomains formed by microphase separation are not stabilized, because the  $T_c$  is higher than the glass transition temperature of PLA block and the melting point of PEO block. As a result, the PEO block is in melt state, and the chain mobility of PLA block is relatively strong. Meanwhile, the inducement time for crystallization at low temperature is quite short, homogeneous nucleation occurs in quite a short time, then a number of small spherulites grow up within a small domain rapidly.

A distinct annealing process named process B was carried out. PEO-*b*-PLA copolymer films were completely melted, and then cooled to 30 °C, which is below the glass transition temperature of PLA block. Five min later, it is heated to  $T_c$  for isothermal crystallization.

Figures 21e–i and 22 show the morphologies of PEO-*b*-PLA copolymers crystallized in hard environment observed at room temperature. Star-shaped (or flower-shaped) morphologies were observed in PLA<sub>16k</sub>-*b*-PEO<sub>5k</sub> and PLA<sub>30k</sub>-*b*-PEO<sub>5k</sub> copolymers shown in Figure 21e–i and 22. No Maltese cross can be seen in the polarized optical microscopy images, and the boundary lines of the two morphologies are not linear but irregularly curvilinear, which both confirm that the morphologies are not spherulites, but a new kind of morphology which has never been reported for PLA and its copolymers.

In order to get detailed information about the peculiar star-shaped morphology, AFM is used, and the typical height and the phase images are shown in Figure 23. It is found that the morphological features are absolutely different from those in melt crystallization shown in Figure 18. The morphologies which are tens of microns or even a hundred microns in size are composed of

lozenge-shaped PLA crystals shown in Figure 23. The size of the lamellae is at the nanometer scale, which is similar to that of the PLA single crystal. The lozenge-shaped lamellae with abundance of screw dislocation were also observed via AFM (shown in Figure 23c). The single crystals orientated along the radical direction and the size of the lozenge-shaped crystals become larger when the  $T_c$  increases (in comparison with those in Figure 23a–c).

**Figure 21.** Morphologies in PLA<sub>16k</sub>-*b*-PEO<sub>5k</sub> copolymer films crystallized at (a) 55 °C; (b) 60 °C; (c) 70 °C; (d) 80 °C from melt state; (e) 110 °C; (f) 115 °C; (g) 120 °C; (h) 125 °C and (i) 130 °C from  $T_g$  of PLA block with heating after quenching from annealing temperature. The bar corresponds to 100  $\mu$ m.

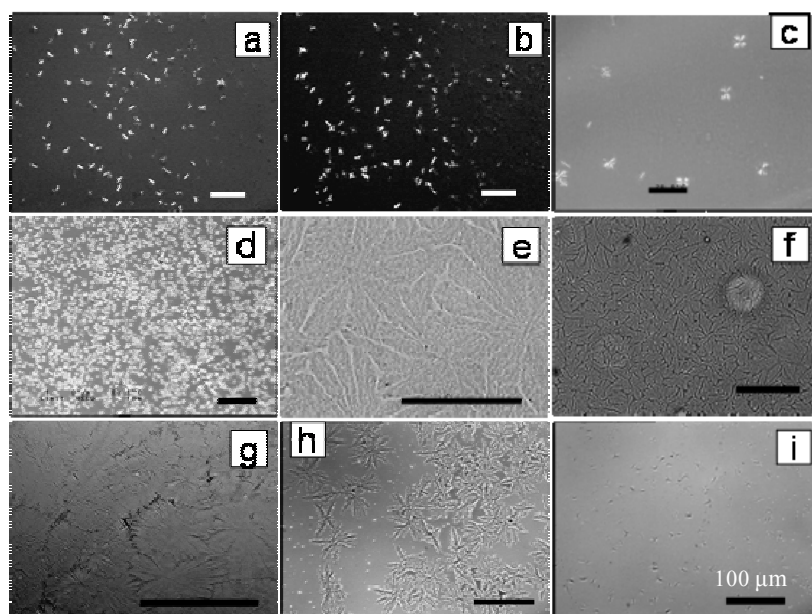


**Figure 22.** Morphologies in PLA<sub>30k</sub>-*b*-PEO<sub>5k</sub> copolymer films crystallized at (a) 110 °C (b) 120 °C from  $T_g$  of PLA block with heating after quenching from annealing temperature. The bar corresponds to 100  $\mu$ m.

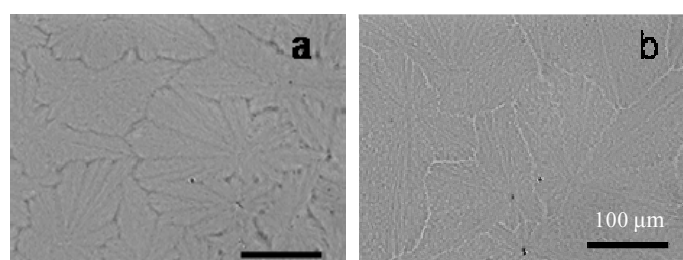
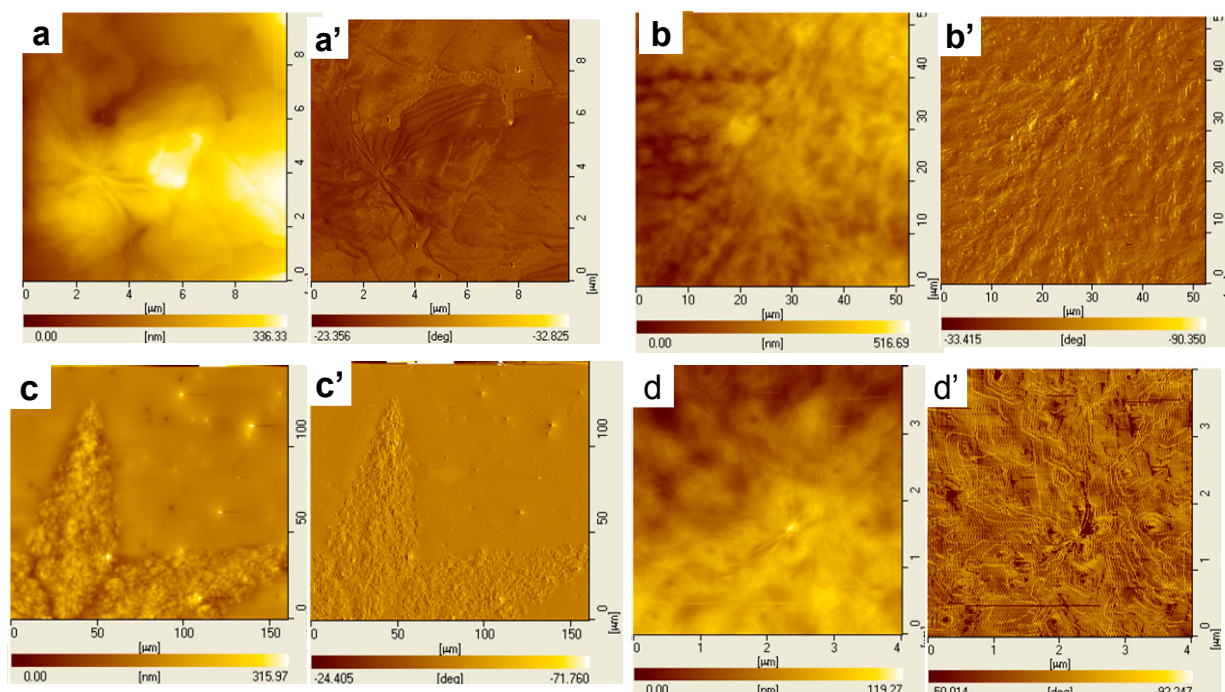


**Figure 23.** AFM images of detailed morphological structures in asymmetric PLA-*b*-PEO copolymer films. PLA<sub>16k</sub>-*b*-PEO<sub>5k</sub>: isothermally crystallized at (a) and (a') 130 °C, (b) and (b') 110 °C, (c) and (c') 125 °C; PLA<sub>30k</sub>-*b*-PEO<sub>5k</sub>: (d) and (d') 110 °C from  $T_g$  of PLA block with heating after quenching from annealing temperature.



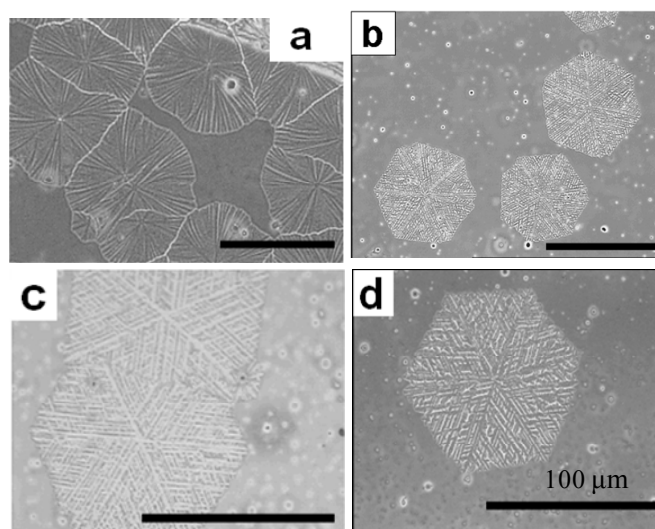
Furthermore, lamellar thickness ( $d$ ) of PLA<sub>16k</sub>-*b*-PEO<sub>5k</sub> copolymer crystallized in a hard environment increases from 18.6 nm at 110 °C, 19.3 nm 125 °C, to 20.5 nm 130 °C. The values of lamellar thickness ( $d$ ) of the copolymers crystallized in a soft confined environment are about 4–6 nm larger than those formed in melt crystallization. Alternate amorphous–crystalline phase structure is formed in both soft and hard confined environments. As a consequence, the lamellar thickness ( $d$ ) evaluated by AFM is the sum of PLA lamellar thickness ( $d_{\text{PLA,c}}$ ) and the amorphous layer thickness ( $d_a$ ). In a soft confined environment, the PLA block and the PEG block are homogeneous or weakly segregated (miscible) in the melt state. As the temperature is decreased, crystallization is the dominating driving force leading to extensive rearrangement of the morphology when the PLA block crystallizes first. During its crystallization, the lamellar thickness increases. After the PLA block crystallizes completely, the lamellar thickness is 12–16 nm, which consists of the lamellar crystal thickness of the PLA block and the thickness of the amorphous PEG layer if the thickness of the amorphous PLA layer is neglected. In a hard confined environment, the immiscibility of PLA and PEO blocks, and vitrification of PLA block during the annealing from the disordered state and isothermal process at 30 °C (even part of PEO block is probably to be crystallized) form a relatively stable layer–layer structure. During the crystallization of PLA after heating from 30 °C, despite the PEO block being completely melted, the microdomain formed by microphase separation confines the crystallization of PLA block and diffusions of PLA and PEO blocks. After PLA block crystallizes completely, the lamellar thickness is 18–20 nm, which consists of the lamellar crystal thickness of the PLA block and the thickness of the amorphous PEG and PLA layer, and the thickness of the amorphous PLA layer cannot be neglected. In a soft confined environment, most of the PEO component may distribute on the surfaces of the

crystalline morphologies driven by the competition between crystallization of PLA and microphase separation. In a hard confined environment, the stabilized microdomains make PEO blocks distribute between the PLA lamellae. As a result, the increase of the lamellar thickness is probably to be ascribed to the increase of thickness of amorphous PEO and PLA layer.

### 3.3. Dendritic Superstructures and Structure Transitions in PEO-*b*-PCL Diblock Copolymers [48]

Optical microscopic images of PLA<sub>16k</sub>-*b*-PEO<sub>5k</sub> copolymer thin films isothermally crystallized at different temperatures for very long times are shown in Figure 24. Dendritic morphologies are formed. At 90 °C shown in Figure 24a, dendritic morphologies with discal contour were observed, which were formed with many radial branches. Dendritic superstructures with hexagonal contour were observed in thin films crystallized above 100 °C, as seen in Figure 24b–d. The images show that the dendritic morphology is composed of six sectors with some overgrowth lamellae. The change of the morphology contour with crystallization temperature shown in Figure 1 is ascribed to the temperature dependence of nucleation and growth, the addition of PEO block, and phase separation between the two unlike blocks during the crystallization of PLA.

**Figure 24.** Morphologies of PLA<sub>16k</sub>-*b*-PEO<sub>5k</sub> copolymer thin films crystallized at (a) 90 °C; (b) 100 °C; (c) 110 °C; and (d) 120 °C. The thickness of the films is  $\sim 220 \pm 30$  nm. The bar corresponds to 100  $\mu$ m. Reprinted with permission from American Chemical Society, 2009 [48].



To visualize the detailed crystalline morphologies of PLA<sub>16k</sub>-*b*-PEO<sub>5k</sub> copolymer, tapping mode AFM was employed. The AFM images are shown in Figure 25. For the thin films crystallized at lower temperatures, the number of the main branch every crystalline morphology is larger than that of identical films crystallized at higher temperatures. Lozenge-spiral dislocation (right arrowed in the phase images at 120 °C), lozenge multilayer (arrowed in the images at 100 °C), or truncated-lozenge multilayer (left arrowed in the images at 120 °C) was formed in the growth direction perpendicular to the lamellae. The size of lamellae increases with crystallization temperature. The d spacing of lamellae 10–12 nm thick is identical with that of the PLA single crystal. The crystalline morphology is formed by stacking flat-on growing lamellae in the thin film. Lozenge-shaped single

crystal with screw dislocation of PLA has been reported in thin film of PLA or its copolymers that the thickness is less than 100 nm [6,7,12,55–57]. However, the special crystalline morphology of hexagonal dendrite stacked with PLA single crystals has never been reported. The dependence of crystalline morphology on  $T_c$  can be explained by supercooling and phase separation. For PLA homopolymer thin films with identical thickness, spherulitic morphologies are formed in the temperature range from 90 to 120 °C. For PEO-*b*-PLA copolymer thin films, microphase separation driven by the crystallization of PLA block formed a layer–layer structure (that is to say alternate PLA- and PEO-rich domains). Furthermore, the size of the PLA layer is quite smaller to the film thickness, which is tens or a hundred nanometers, as determined by AFM. At lower  $T_c$ , the supercooling is larger and many nucleus are formed rapidly. Subsequently, many small PLA single crystals grow and star-shaped dendritic morphologies are observed at 90 °C in Figures 24a and 25a. While at a higher  $T_c$ , the number of elementary nucleuses is relatively small; secondary nucleation is therefore important in the crystallization process. As a consequence, dendritic morphologies composed with main-branches, secondary side-branches and tertiary side-branches were formed shown in Figures 24b–d and 25b–d. Furthermore, the structure in the areas of the films that appear not to contain dendritic structures was amorphous PEO and PLA blocks. At high crystallization temperatures, it is difficult for nucleation, especially for homogeneous nucleation. Once the nucleus was formed, crystallization procedures begin by diffusion and ordering of PLA chains. In the crystallization process, the PLA block can preferentially attach to the growth front, and then the accumulation of amorphous components in the vicinity of the dendrites will prevent the nucleation and crystallization in the areas.

Figure 26 shows typical optical microscope (OM) images of PLA<sub>16k</sub>-*b*-PEO<sub>5k</sub> thin films with different thicknesses crystallized at 110 °C. Spherulites are formed in ~10 μm thick films as shown in Figure 26a, while for the films in the thickness range from 1 to ~200 nm, dendritic morphologies were observed, as seen in Figure 26b–e. Maltese cross extinction was not found in the center of any crystalline morphology in the films with the thickness range from 1 to ~200 nm, indicating that the optic axis (the chain axis) is normal to the plane of the film. The morphologies in Figure 26b–e are discal dendritic as confirmed from AFM observations. Most of their fringe frame of the morphologies formed in thin films with the thickness from 200 to 400 nm are hexagonal as shown in Figure 26c–e, and the size of the hexagonal morphologies is about 100 μm. The hexagonal dendritic morphologies were composed of six sectors. In the film with 115 nm thickness (Figure 26f), lozenge-shaped lamellae were formed. The stack and the growth of PLA single crystals are oriented, as shown in Figure 26f. The diffusion and crystallization processes of PLA block drove microphase separation between the unlike blocks, and the formation of concentration gradient of PLA. Moreover, the average growth rate was nearly linear, and it was easy to form dendritically and not spherulitically in thin film. As a result, the hexagonal contour morphology was likely formed. The formation of the dendritic morphologies stacked with PLA single crystals in PEO-*b*-PLA thin films ranging from 1 to 200 nm thick is related with the phase structure and its evaluation during the crystallization process, and the mechanism will be further discussed in the following paragraph.

**Figure 25.** AFM height (left column) and phase (right column) images of PLA<sub>16k</sub>-*b*-PEO<sub>5k</sub> copolymer thin films crystallized at (a) and (a') 90 °C; (b) and (b') 100 °C; (c) and (c') 110 °C; (d) and (d') 120 °C; and (e) and (e') 110 °C, A: the main branch; B: the secondary side-branch; C: the tertiary side-branch. Reprinted with permission from American Chemical Society, 2009 [48].

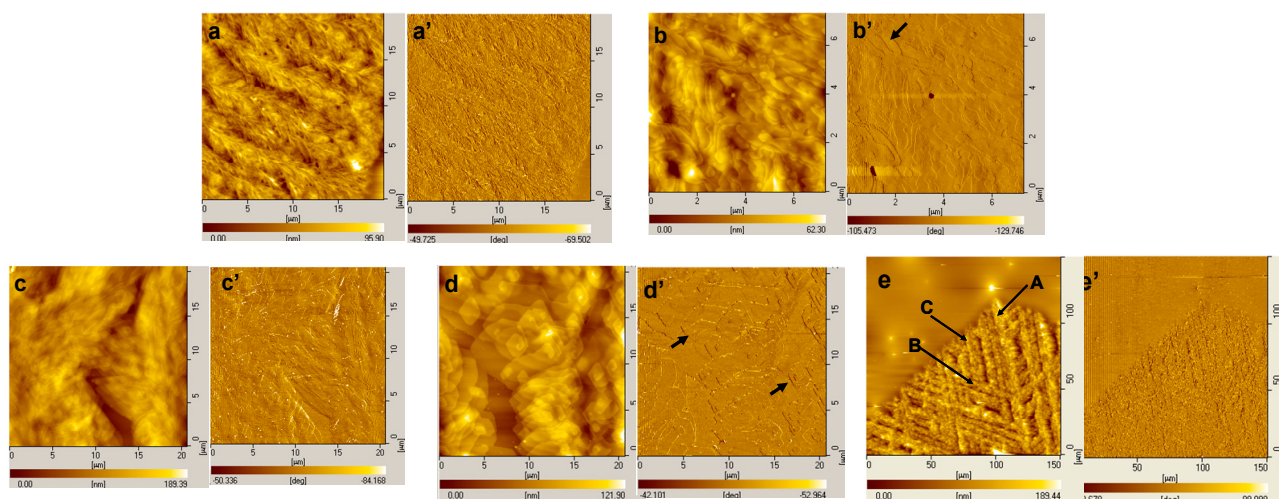


**Figure 26.** Morphologies of PLA<sub>16k</sub>-*b*-PEO<sub>5k</sub> copolymer thin films crystallized at 110 °C. Film thickness: (a) ~10 μm; (b) 1 μm; (c) ~400 nm; (d) ~300 nm; (e) 220 nm; and (f) 115 nm. The bar corresponds to 100 μm. Reprinted with permission from American Chemical Society, 2009 [48].

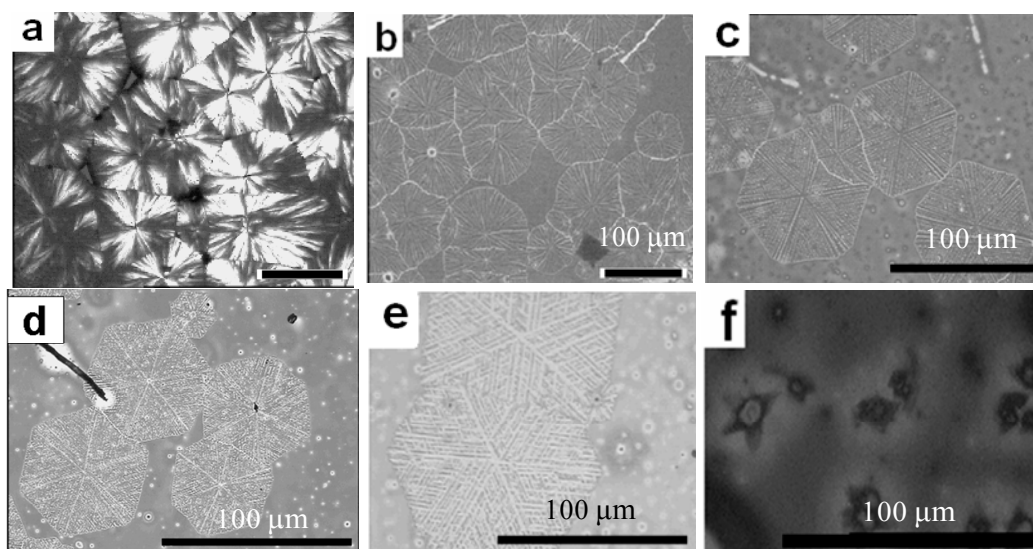
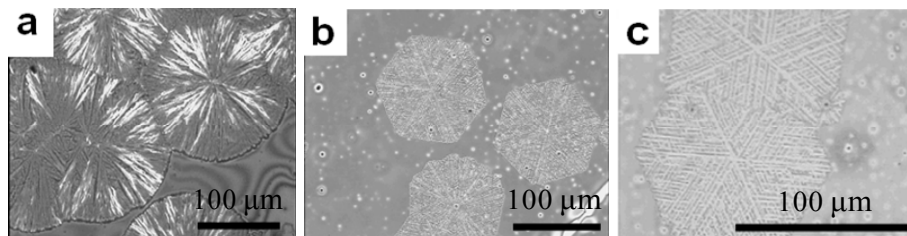


Figure 27 shows the effect of the component on crystalline morphology. It can be seen that the morphology changes from spherulite (Figure 27a) to dendrite (Figure 27b), to dendrite with hexagonal contour (Figure 27c) with the volume fraction of PEO increasing. The effect of PEO blocks on the crystallization and morphological behaviors of PLA blocks is multiple. The melting points of PLA block in PEO-*b*-PLA copolymers decrease with its fraction decreased, so the degree of supercooling ( $\Delta T = T_m - T_c$ ) decreases with PEO fraction increase. Subsequently, at 110 °C, it is a low temperature range of crystallization for PLA homopolymer, and a spherulite is formed (Figure 27a), while for PLA<sub>30k</sub>-*b*-PEO<sub>5k</sub> and PLA<sub>16k</sub>-*b*-PEO<sub>5k</sub> copolymers, it is a high temperature range of crystallization, and

dendritic morphologies are observed (Figure 27b,c). It is common to form a dendritic morphology in thin film, and this has been previously discussed. Meanwhile, the volume fractions of PLA block and the total degree of polymerization ( $N$ ) are different in the three samples in Figure 27a–c; the segregated strength of microphase separation between the two blocks is different. As a result, the number of nucleus of every area, and the density of the branches in PLA<sub>30k</sub>-*b*-PEO<sub>5k</sub> copolymer thin film, are larger than that in PLA<sub>16k</sub>-*b*-PEO<sub>5k</sub>. That is to say, as the volume fraction of PEO block increases, the effect of PEO on the crystalline morphology also increases. It affects the crystallization of PLA block in three ways. First, the number of PLA blocks decreases in thin film of the same thickness. Second, the diffusion of PLA block becomes more difficult because of the increase of the volume fraction of PEO. Third, the size of microstructure driven by phase separation may be larger. As a consequence, we obtained the evolution of crystalline morphology in copolymer thin films with a different component in Figure 27. The morphologies were observed after annealed to room temperature. As a result, the PEO blocks might also crystallize, but the wide-angle X-ray diffraction (WAXD) research has confirmed that it is quite difficult for PEO block to crystallize in such asymmetric block copolymers because of the strong confinement from microphase separation.

**Figure 27.** Morphologies of (a) PLA<sub>31k</sub> homopolymer; (b) PLA<sub>30k</sub>-*b*-PEO<sub>5k</sub>; and (c) PLA<sub>16k</sub>-*b*-PEO<sub>5k</sub> copolymer films with the thickness of  $\sim 220 \pm 30$  nm crystallized at 110 °C. The bar corresponds to 100  $\mu$ m. Reprinted with permission from American Chemical Society, 2009 [48].



It is not certain whether the crystalline morphologies observed by OM and AFM in Figures 24–27 are those created during crystallization of PLA block. It is possible that some of the patterns are formed by rearrangements after crystallization (or rearrangements of already crystallized parts while new material is still crystallizing. In order to confirm whether the morphologies observed are those formed during crystallization or not, *in situ* OM experimentation for isothermal crystallization was carried out. Figure 28 shows the polarized optical microscopic images of morphological growth of PLA<sub>16k</sub>-PEO<sub>5k</sub> copolymer thin film isothermally crystallized at 110 °C. At 12 min, as shown in Figure 28a, the similar dendritic morphologies with hexagonal contour as those in Figures 24 and 26 are observed. From Figure 28b–d, the thickness and the size of the crystalline morphologies grew thicker and larger, but the crystalline morphology observed by OM is remains the same the entire time, indicating the morphologies observed are created during crystallization.

The thickness of copolymer film in the experiment is 1  $\mu$ m~200 nm; as a result, the substrate may influence the crystalline morphology. It is possible that one of the blocks adsorbs strongly to the substrate. If this is the case, then the strong attachment of one block to the substrate can control the morphology. PEO-*b*-PLA copolymers and PLA/PEO blends belong to a weakly segregated system,

PEO and PLA could not be strongly segregated or one of them strongly adsorbed to the substrate. Meanwhile, the film thickness range from 1  $\mu\text{m}$  to 200 nm is much larger than the size of the extended copolymer chain, so the effect of substrate on the morphology is negligible.

**Figure 28.** Polarized optical microscopic images of PLA<sub>16k</sub>-PEO<sub>5k</sub> thin films crystallized at 110 °C at (a) 12 min; (b) 18 min; (c) 28 min; and (d) 49 min after being completely melted at 180 °C. The bar corresponds to 100  $\mu\text{m}$ . Reprinted with permission from American Chemical Society, 2009 [48].

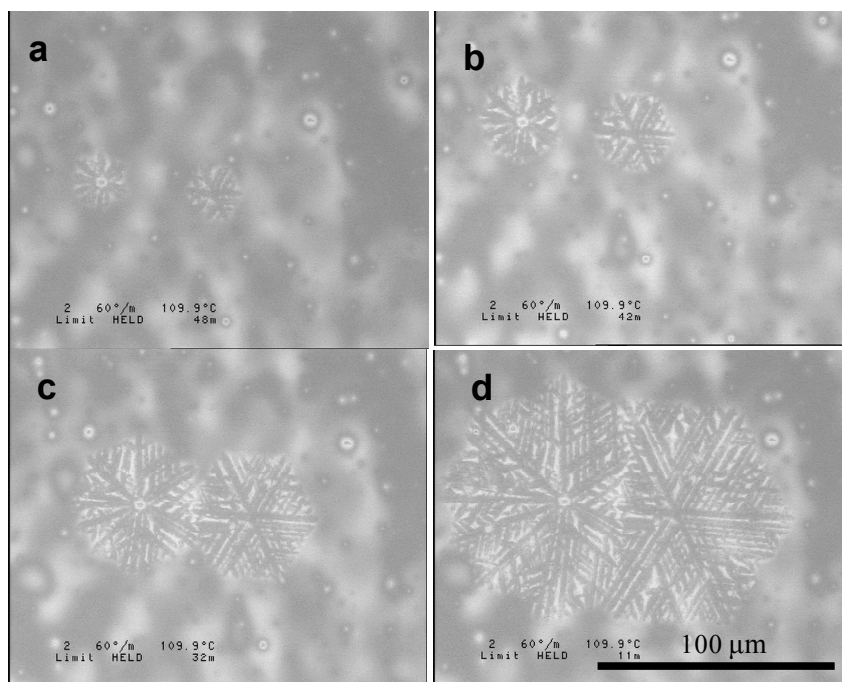
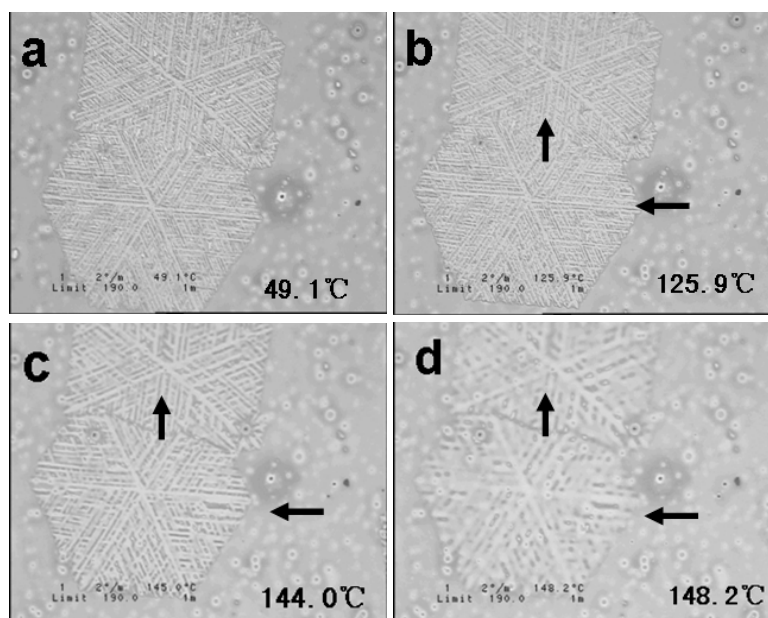


Figure 29 shows the time-dependent changes in surface morphology of PEO-*b*-PLA thin films with 220 nm thickness during isothermal crystallization at 110 °C. At 125.9 °C, the sectors labeled by arrows in Figure 29b started melting, when the temperature reached 144 °C, as shown in Figure 29c. The sectors next to the labeled ones began to melt, and at 148.9 °C in Figure 29d, the sectors labeled with arrows obfuscated the crystalline morphology, while clarity in the sectors next to the labeled ones indicated that the thermal-stability of the sectors were different.

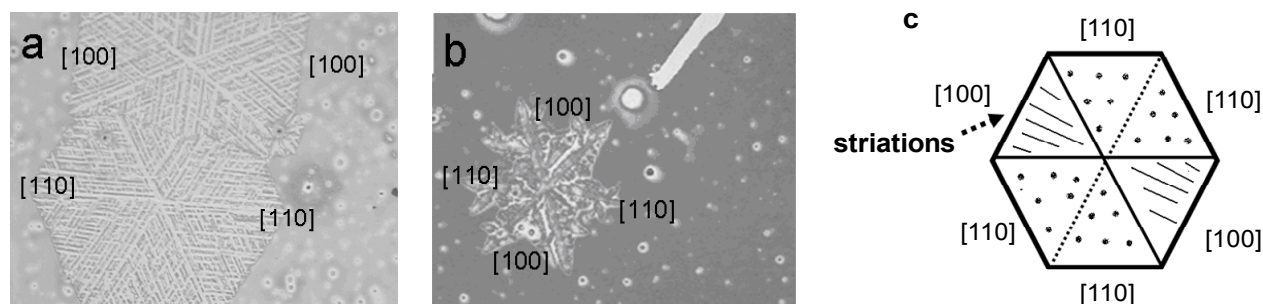
For PLA crystals grown in spin-coated thin films on solid surfaces, four symmetrically disordered sectors in the hexagonal superstructure are formed. They can be classified into two sectors, (100) and (110), in terms of chain folding and crystal growth directions. From the growth process in Figure 29 and the dendritic morphologies with hexagonal contour formed in thin film with ~200–400 nm thickness in Figures 24–26, the hexagonal superstructure is composed of two different sectors shown in Figure 30a,b. Figure 30c's schematic represents the hexagonal morphology. In the sector (110) growth plane, the chain-folding direction is the same as the crystal growth direction. On the other hand, the chain-folding direction in the sectors with a (100) growth plane alternates between (110) sectors. In the case of PLA thin film, the sectors with (100) growth plane showed some striations, they are along the main-branches and parallel with each other, the striations are nearly perpendicular to the

crystal growth face, suggesting that the disordered chain (amorphous PLA and PEO phase) packing exists in addition to the chain-folding instability.

**Figure 29.** Optical micrographs of the melting process of PLA<sub>16k</sub>-*b*-PEO<sub>5k</sub> thin film (~220 nm thick, isothermally crystallized at 110 °C). Reprinted with permission from American Chemical Society, 2009 [48].



**Figure 30.** Two types of sectors, (110) and (100), were classified in terms of chain-folding and crystal growth directions in hexagonal superstructure of PLA-*b*-PEO copolymer thin films isothermally crystallized at (a) 110 °C and (b) 125 °C. (c) Schematic representation of the hexagonal superstructure of PLA-*b*-PEO copolymer thin film. Reprinted with permission from American Chemical Society, 2009 [48].



#### 4. Summary and Outlook

Competition of crystallization and microphase separation, and/or other driving force can lead to more abundant structures for BCCPs. The unique structures and morphologies resulting from break-out and confined crystallization, controlled growth of thin film crystallization, eutectic crystal of double crystalline blocks, stereocomplexation of enantiomeric isomers, and micelles with a crystalline core, can be observed for block copolymers. The structures and morphologies of semicrystalline BCCPs in bulk material have been extensively studied and well understood in different kinds of block copolymers.

Studies on the relationship among the chemical composition, macromolecular architectures, thermal history, physical properties, mechanical performance, biodegradability and biocompatibility of BBCPs are frequently neglected. Meanwhile, the controlled nano-scale structures, the orientation of lamellar crystals, the relationship between structure and function of BBCPs, crystallization kinetics in thin films, confined crystallization from crystal lamellae and glass state should be more thoroughly studied. Controlled growth and micro-structure, and growth kinetics of semicrystalline micelles of BBCPs are of importance for applications in the biomedical area, and should be extensively studied.

### Acknowledgments

This work was supported by the National Natural Science Foundation of China (20974077 and 20574069).

### Author Contributions

Feifei Xue prepared the manuscript including published papers of her work. All of the results in present review are publications of Shichun Jiang's group.

### Conflicts of Interest

The authors declare no conflict of interest.

### References

1. Hamley, I. *Interfaces Crystallization Viscoelasticity*; Springer: Berlin, Germany, 1999; p. 113.
2. Müller, A.J.; Balsamo, V.; Arnal, M.L. *Block Copolymers II*; Springer: Berlin, Germany, 2005; p. 1.
3. Muthukumar, M.; Ober, C.; Thomas, E.L. Competing interactions and levels of ordering in self-organizing polymeric materials. *Science* **1997**, *277*, 1225–1232.
4. Ryan, A.J.; Hamley, I.W.; Bras, W.; Bates, F.S. Structure development in semicrystalline diblock copolymers crystallizing from the ordered melt. *Macromolecules* **1995**, *28*, 3860–3868.
5. Rangarajan, P.; Register, R.A.; Fetters, L.J.; Bras, W.; Naylor, S.; Ryan, A.J. Crystallization of a Weakly Segregated Polyolefin Diblock Copolymer. *Macromolecules* **1995**, *28*, 4932–4938.
6. Sun, J.; Hong, Z.; Yang, L.; Tang, Z.; Chen, X.; Jing, X. Study on crystalline morphology of poly(L-lactide)-poly(ethylene glycol) diblock copolymer. *Polymer* **2004**, *45*, 5969–5977.
7. Huang, S.; Jiang, S.; An, L.; Chen, X. Crystallization and morphology of poly(ethylene oxide-*b*-lactide) crystalline–crystalline diblock copolymers. *J. Polym. Sci. B Polym. Phys.* **2008**, *46*, 1400–1411.
8. Södergård, A.; Stolt, M. Properties of lactic acid based polymers and their correlation with composition. *Prog. Polym. Sci.* **2002**, *27*, 1123–1163.
9. Uhrich, K.E.; Cannizzaro, S.M.; Langer, R.S.; Shakesheff, K.M. Polymeric systems for controlled drug release. *Chem. Rev.* **1999**, *99*, 3181–3198.
10. Bates, F.S.; Fredrickson, G.H. Block copolymer thermodynamics: Theory and experiment. *Ann. Rev. Phys. Chem.* **1990**, *41*, 525–557.

11. Zhu, L.; Cheng, S.Z.; Calhoun, B.H.; Ge, Q.; Quirk, R.P.; Thomas, E.L.; Hsiao, B.S.; Yeh, F.; Lotz, B. Crystallization temperature-dependent crystal orientations within nanoscale confined lamellae of a self-assembled crystalline–amorphous diblock copolymer. *J. Am. Chem. Soc.* **2000**, *122*, 5957–5967.
12. Müller, A.J.; Arnal, M.L.; Balsamo, V. *Progress in Understanding of Polymer Crystallization*; Springer: Berlin, Germany, 2007; p. 229.
13. Rangarajan, P.; Register, R.A.; Adamson, D.H.; Fetters, L.J.; Bras, W.; Naylor, S.; Ryan, A.J. Dynamics of structure formation in crystallizable block copolymers. *Macromolecules* **1995**, *28*, 1422–1428.
14. Nojima, S.; Kato, K.; Yamamoto, S.; Ashida, T. Crystallization of block copolymers. 1. Small-angle X-ray scattering study of a  $\epsilon$ -caprolactone-butadiene diblock copolymer. *Macromolecules* **1992**, *25*, 2237–2242.
15. Reiter, G.; Castelein, G.; Sommer, J.-U.; Röttele, A.; Thurn-Albrecht, T. Direct visualization of random crystallization and melting in arrays of nanometer-size polymer crystals. *Phys. Rev. Lett.* **2001**, *87*, doi:10.1103/PhysRevLett.87.226101.
16. Hamley, I.; Castelletto, V.; Castillo, R.V.; Müller, A.J.; Martin, C.; Pollet, E.; Dubois, P. Crystallization in poly(L-lactide)-*b*-poly( $\epsilon$ -caprolactone) double crystalline diblock copolymers: A study using X-ray scattering, differential scanning calorimetry, and polarized optical microscopy. *Macromolecules* **2005**, *38*, 463–472.
17. Nojima, S.; Toei, M.; Hara, S.; Tanimoto, S.; Sasaki, S. Size dependence of crystallization within spherical microdomain structures. *Polymer* **2002**, *43*, 4087–4090.
18. Joncheray, T.J.; Denoncourt, K.M.; Meier, M.A.; Schubert, U.S.; Duran, R.S. Two-dimensional self-assembly of linear poly(ethylene oxide)-*b*-poly( $\epsilon$ -caprolactone) copolymers at the air–water interface. *Langmuir* **2007**, *23*, 2423–2429.
19. Naolou, T.; Busse, K.; Lechner, B.-D.; Kressler, J. The behavior of poly ( $\epsilon$ -caprolactone) and poly (ethylene oxide)-*b*-poly ( $\epsilon$ -caprolactone) grafted to a poly (glycerol adipate) backbone at the air/water interface. *Colloid Polym. Sci.* **2014**, *292*, 1199–1208.
20. Jiang, S.; He, C.; An, L.; Chen, X.; Jiang, B. Crystallization and ring-banded spherulite morphology of poly(ethylene oxide)-*block*-poly( $\epsilon$ -caprolactone) diblock copolymer. *Macromol. Chem. Phys.* **2004**, *205*, 2229–2234.
21. Keith, H.D. Banding in spherulites: two recurring topics. *Polymer* **2001**, *42*, 09987–09993.
22. Keith, H.D.; Padden, F.J., Jr. Banding in polyethylene and other spherulites. *Macromolecules* **1996**, *29*, 7776–7786.
23. Keith, H.D.; Padden, F.J., Jr.; Russell, T.P. Morphological changes in polyesters and polyamides induced by blending with small concentrations of polymer diluents. *Macromolecules* **1989**, *22*, 666–675.
24. Keith, H.D.; Padden, F.J., Jr. Twisting orientation and the role of transient states in polymer crystallization. *Polymer* **1984**, *25*, 28–42.
25. Saracovan, I.; Keith, H.D.; Manley, R.S.J.; Brown, G.R. Banding in spherulites of polymers having uncompensated main-chain chirality. *Macromolecules* **1999**, *32*, 8918–8922.
26. Wang, Z.G.; Wang, X.; Yu, D.; Jiang, B. The formation of ring-banded spherulites of poly( $\epsilon$ -caprolactone) in its miscible mixtures with poly(styrene-co-acrylonitrile). *Polymer* **1997**, *38*, 5897–5901.

27. Lotz, B.; Thierry, A. Spherulite morphology of form III isotactic poly(L-butene). *Macromolecules* **2003**, *36*, 286–290.
28. Bogdanov, B.; Vidts, A.; Schacht, E.; Berghmans, H. Isothermal crystallization of poly( $\epsilon$ -caprolactone–ethylene glycol) block copolymers. *Macromolecules* **1999**, *32*, 726–731.
29. Jiang, S.; He, C.; Men, Y.; Chen, X.; An, L.; Funari, S.S.; Chan, C.-M. Study of temperature dependence of crystallisation transitions of a symmetric PEO-PCL diblock copolymer using simultaneous SAXS and WAXS measurements with synchrotron radiation. *Eur. Phys. J. E* **2008**, *27*, 357–364.
30. Nojima, S.; Ito, K.; Ikeda, H. Composition dependence of crystallized lamellar morphology formed in crystalline–crystalline diblock copolymers. *Polymer* **2007**, *48*, 3607–3611.
31. Nojima, S.; Kiji, T.; Ohguma, Y. Characteristic melting behavior of double crystalline poly( $\epsilon$ -caprolactone)-*block*-polyethylene copolymers. *Macromolecules* **2007**, *40*, 7566–7572.
32. Nojima, S.; Akutsu, Y.; Akaba, M.; Tanimoto, S. Crystallization behavior of poly( $\epsilon$ -caprolactone) blocks starting from polyethylene lamellar morphology in poly( $\epsilon$ -caprolactone)-*block*-polyethylene copolymers. *Polymer* **2005**, *46*, 4060–4067.
33. Meng, F.; Hiemstra, C.; Engbers, G.H.M.; Feijen, J. Biodegradable polymersomes. *Macromolecules* **2003**, *36*, 3004–3006.
34. Cerrai, P.; Tricoli, M.; Andruzzi, F.; Paci, M.; Paci, M. Polyether-polyester block copolymers by non-catalysed polymerization of  $\epsilon$ -caprolactone with poly(ethylene glycol). *Polymer* **1989**, *30*, 338–343.
35. Perret, R.; Skoulios, A. Synthèse et caractérisation de copolymères séquencés polyoxyéthylène/poly- $\epsilon$ -caprolactone. *Makromol. Chem.* **1972**, *156*, 143–156. (In Germany)
36. Wang, Z.-G.; Hsiao, B.S.; Sirota, E.B.; Agarwal, P.; Srinivas, S. Probing the early stages of melt crystallization in polypropylene by simultaneous small- and wide-angle X-ray scattering and laser light scattering. *Macromolecules* **2000**, *33*, 978–989.
37. Xue, F.; Chen, X.; An, L.; Funari, S.S.; Jiang, S. Soft nanoconfinement effects on the crystallization behavior of asymmetric poly(ethylene oxide)-*block*-poly( $\epsilon$ -caprolactone) diblock copolymers. *Polym. Int.* **2012**, *61*, 909–917.
38. Hamley, I.W. Solid state structure of block copolymers. In *The Physics of Block Copolymers*; Oxford University Press: New York, NY, USA, 1998.
39. Harkless, C.R.; Singh, M.A.; Nagler, S.E.; Stephenson, G.B.; Jordan-Sweet, J.L. Small-angle X-ray-scattering study of ordering kinetics in a block copolymer. *Phys. Rev. Lett.* **1990**, *64*, doi:10.1103/PhysRevLett.64.2285.
40. Oono, Y.; Bahiana, M.  $\frac{2}{3}$ -Power law for copolymer lamellar thickness implies a  $\frac{1}{3}$ -power law for spinodal decomposition. *Phys. Rev. Lett.* **1988**, *61*, doi: 10.1103/PhysRevLett.61.1109.
41. Hashimoto, T.; Kowsaka, K.; Shibayama, M.; Suehiro, S. Time-resolved small-angle X-ray scattering studies on the kinetics of the order-disorder transition of block polymers. 1. Experimental technique. *Macromolecules* **1986**, *19*, 750–754.
42. Hashimoto, T.; Kowsaka, K.; Shibayama, M.; Kawai, H. Time-resolved small-angle x-ray scattering studies on the kinetics of the order-disorder transition of block polymers. 2. Concentration and temperature dependence. *Macromolecules* **1986**, *19*, 754–762.

43. Xue, F.-F.; Chen, X.-S.; An, L.-J.; Funari, S.S. Confined lamella formation in crystalline-crystalline poly(ethylene oxide)-*b*-poly( $\epsilon$ -caprolactone) diblock copolymers. *Chin. J. Polym. Sci.* **2013**, *31*, 1260–1270.
44. Yasuniwa, M.; Tsubakihara, S.; Iura, K.; Ono, Y.; Dan, Y.; Takahashi, K. Crystallization behavior of poly(L-lactic acid). *Polymer* **2006**, *47*, 7554–7563.
45. Xu, J.; Guo, B.-H.; Zhou, J.-J.; Li, L.; Wu, J.; Kowalczyk, M. Observation of banded spherulites in pure poly(L-lactide) and its miscible blends with amorphous polymers. *Polymer* **2005**, *46*, 9176–9185.
46. Maillard, D.; Prud' Homme, R.E. Crystallization of ultrathin films of polylactides: From chain chirality to lamella curvature and twisting. *Macromolecules* **2008**, *41*, 1705–1712.
47. Tsuji, H.; Tezuka, Y.; Saha, S.K.; Suzuki, M.; Itsuno, S. Spherulite growth of L-lactide copolymers: Effects of tacticity and comonomers. *Polymer* **2005**, *46*, 4917–4927.
48. Huang, S.; Jiang, S.; Chen, X.; An, L. Dendritic superstructures and structure transitions of asymmetric poly(L-lactide-*b*-ethylene oxide) diblock copolymer thin films. *Langmuir* **2009**, *25*, 13125–13132.
49. Zhang, J.; Tashiro, K.; Tsuji, H.; Domb, A.J. Disorder-to-order phase transition and multiple melting behavior of poly(L-lactide) investigated by simultaneous measurements of WAXD and DSC. *Macromolecules* **2008**, *41*, 1352–1357.
50. Cho, T.-Y.; Strobl, G. Temperature dependent variations in the lamellar structure of poly(L-lactide). *Polymer* **2006**, *47*, 1036–1043.
51. Zhang, J.; Duan, Y.; Sato, H.; Tsuji, H.; Noda, I.; Yan, S.; Ozaki, Y. Crystal modifications and thermal behavior of poly(L-lactic acid) revealed by infrared spectroscopy. *Macromolecules* **2005**, *38*, 8012–8021.
52. Di Lorenzo, M.L. Determination of spherulite growth rates of poly(L-lactic acid) using combined isothermal and non-isothermal procedures. *Polymer* **2001**, *42*, 9441–9446.
53. Abe, H.; Kikkawa, Y.; Inoue, Y.; Doi, Y. Morphological and kinetic analyses of regime transition for poly[(S)-lactide] crystal growth. *Biomacromolecules* **2001**, *2*, 1007–1014.
54. Mijovic, J.; Sy, J.-W. Molecular dynamics during crystallization of poly(L-lactic acid) as studied by broad-band dielectric relaxation spectroscopy. *Macromolecules* **2002**, *35*, 6370–6376.
55. Yang, J.; Zhao, T.; Zhou, Y.; Liu, L.; Li, G.; Zhou, E.; Chen, X. Single crystals of the poly(L-lactide) block and the poly(ethylene glycol) block in poly(L-lactide)–poly(ethylene glycol) diblock copolymer. *Macromolecules* **2007**, *40*, 2791–2797.
56. Kikkawa, Y.; Abe, H.; Iwata, T.; Inoue, Y.; Doi, Y. In situ observation of crystal growth for poly[(S)-lactide] by temperature-controlled atomic force microscopy. *Biomacromolecules* **2001**, *2*, 940–945.
57. Fujita, M.; Doi, Y. Annealing and melting behavior of poly(L-lactic acid) single crystals as revealed by in situ atomic force microscopy. *Biomacromolecules* **2003**, *4*, 1301–1307.